

2

**AD-A261 154**



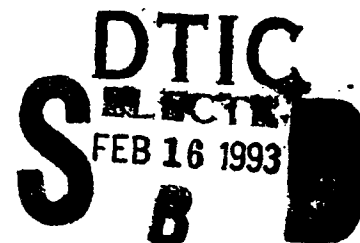
AEROSPACE REPORT NO.  
TR-0091(6925-11)-2

# Analysis of Transient Photoluminescence Measurements on GaAs and AlGaAs Double Heterostructures

Prepared by

D. C. MARVIN, S. C. MOSS, and L. F. HALLE  
Electronics Technology Center  
Technology Operations

13 January 1993



Prepared for

SPACE AND MISSILE SYSTEMS CENTER  
AIR FORCE SYSTEMS COMMAND  
Los Angeles Air Force Base  
P. O. Box 92960  
Los Angeles, CA 90009-2960

Engineering and Technology Group

**93-02848**



THE AEROSPACE CORPORATION  
El Segundo, California

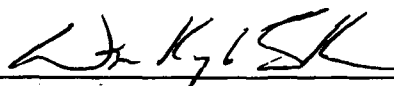
APPROVED FOR PUBLIC RELEASE;  
DISTRIBUTION UNLIMITED

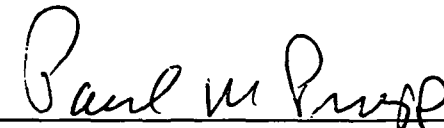
93 2 12 166

This report was submitted by The Aerospace Corporation, El Segundo, CA 90245-4691, under Contract No. F04701-88-C-0089 with the Space and Missile Systems Center, P. O. Box 92960, Los Angeles, CA 90009-2960. It was reviewed and approved for The Aerospace Corporation by B. K. Janousek, Principal Director, Electronics Technology Center. Paul Propp was the project officer for the Mission-Oriented Investigation and Experimentation (MOIE) program.

This report has been reviewed by the Public Affairs Office (PAS) and is releasable to the National Technical Information Service (NTIS). At NTIS, it will be available to the general public, including foreign nationals.

This technical report has been reviewed and is approved for publication. Publication of this report does not constitute Air Force approval of the report's findings or conclusions. It is published only for the exchange and stimulation of ideas.

  
W. Kyle Sneddon, Captain, USAF  
MOIE Program Manager

  
Paul Propp  
Wright Laboratory West Coast Office

UNCLASSIFIED

SECURITY CLASSIFICATION OF THIS PAGE

## REPORT DOCUMENTATION PAGE

1a. REPORT SECURITY CLASSIFICATION Unclassified			1b. RESTRICTIVE MARKINGS		
2a. SECURITY CLASSIFICATION AUTHORITY			3. DISTRIBUTION/AVAILABILITY OF REPORT Approved for public release; distribution unlimited		
2b. DECLASSIFICATION/DOWNGRADING SCHEDULE					
4. PERFORMING ORGANIZATION REPORT NUMBER(S) TR-0091(6925-11)-2			5. MONITORING ORGANIZATION REPORT NUMBER(S) SMC-TR-93-03		
6a. NAME OF PERFORMING ORGANIZATION The Aerospace Corporation Technology Operations		6b. OFFICE SYMBOL (if applicable)	7a. NAME OF MONITORING ORGANIZATION Space and Missile Systems Center		
6c. ADDRESS (City, State, and ZIP Code) El Segundo, CA 90245-4691			7b. ADDRESS (City, State, and ZIP Code) Los Angeles Air Force Base Los Angeles, CA 90009-2960		
8a. NAME OF FUNDING/SPONSORING ORGANIZATION		8b. OFFICE SYMBOL (if applicable)	9. PROCUREMENT INSTRUMENT IDENTIFICATION NUMBER F04701-88-C-0089		
8c. ADDRESS (City, State, and ZIP Code)			10. SOURCE OF FUNDING NUMBERS		
			PROGRAM ELEMENT NO.	PROJECT NO.	TASK NO.
11. TITLE (Include Security Classification) Analysis of Transient Photoluminescence Measurements on GaAs and AlGaAs Double Heterostructures					
12. PERSONAL AUTHOR(S) Marvin, Dean C.; Moss, Steven C.; and Halle, Linda F.					
13a. TYPE OF REPORT		13b. TIME COVERED FROM _____ TO _____		14. DATE OF REPORT (Year, Month, Day) 1993 January 13	
15. PAGE COUNT 54					
16. SUPPLEMENTARY NOTATION					
17. COSATI CODES			18. SUBJECT TERMS (Continue on reverse if necessary and identify by block number)		
FIELD	GROUP	SUB-GROUP			
19. ABSTRACT (Continue on reverse if necessary and identify by block number) <p>We discuss the analysis of transient photoluminescence measurements and the extraction of carrier recombination lifetimes in GaAs and AlGaAs double heterostructures. In contrast to recently reported claims, we demonstrate that even in regions where the measured decay curves show single exponential behavior, the slopes do not, in general, correspond to any single physical carrier lifetime, such as the minority carrier lifetime. A series of measurements over a range of incident optical intensities is required to extract such lifetimes.</p>					
20. DISTRIBUTION/AVAILABILITY OF ABSTRACT <input type="checkbox"/> UNCLASSIFIED/UNLIMITED <input checked="" type="checkbox"/> SAME AS RPT. <input type="checkbox"/> DTIC USERS			21. ABSTRACT SECURITY CLASSIFICATION Unclassified		
22a. NAME OF RESPONSIBLE INDIVIDUAL			22b. TELEPHONE (Include Area Code)		22c. OFFICE SYMBOL

## PREFACE

The authors gratefully acknowledge the support and encouragement of W. C. Hwang and J. A. Gelbwachs.

DTIC QUALITY INSPECTED 3

Accession For	
NTIS SPA&I	<input checked="checked" type="checkbox"/>
DTIC TAB	<input type="checkbox"/>
Unannounced	<input type="checkbox"/>
Justification	
By	
Distribution/	
Availability Codes	
Dist	Avail and/or Special
A-1	

## CONTENTS

PREFACE .....	1
I. INTRODUCTION .....	7
II. SIMULATION METHODS .....	13
A. One-Dimensional Computer Simulation .....	13
B. Recombination Effects Model .....	29
C. Recombination Rate Analysis .....	31
III. DISCUSSION .....	41
IV. CONCLUSIONS .....	47
REFERENCES .....	49
APPENDIX: SIGNAL-TO-NOISE RATIO AND DYNAMIC RANGE OF TRANSIENT PHOTOLUMINESCENCE MEASUREMENTS AT LARGE SPOT SIZE AND LOW EXCITATION LEVEL .....	51

## FIGURES

1.	Typical transient photoluminescence decay curve of a GaAs double heterostructure showing emission intensity, in counts, as a function of time .....	8
2.	Transient photoluminescence decay measurements at excitation intensities increasing from (a) to (d) .....	11
3.	Lifetime extracted from TD2 of the measurements in Figure 2 .....	11
4.	Energy level diagram for the Shockley-Read-Hall recombination process at different limiting excitation intensities .....	16
5.	Calculated band-to-band recombination rate, integrated over sample thickness, as function of time for GaAs double heterostructure .....	19
6.	Results of one-dimensional simulations of integrated band-to-band recombination in 15 $\mu\text{m}$ thick $\text{Al}_x\text{Ga}_{1-x}\text{As}$ double heterostructures for excitation energies of 0.1 nJ, 400 nJ, and 4000 nJ .....	22
7.	Results of one-dimensional simulations of integrated band-to-band recombination in 5 $\mu\text{m}$ thick $\text{Al}_x\text{Ga}_{1-x}\text{As}$ double heterostructures for excitation energies of 0.1 nJ, 400 nJ, and 4000 nJ .....	25
8.	Results of one-dimensional simulations of integrated band-to-band recombination in 5 $\mu\text{m}$ thick $\text{Al}_{0.08}\text{Ga}_{0.92}\text{As}$ double heterostructures at energies of 0.1 nJ, 1 nJ, 5 nJ, 10 nJ, and 50 nJ .....	27
9.	Simulated band-to-band recombination rate in GaAs double heterostructure, assuming uniform distribution of generated carriers and ignoring band-to-band recombination .....	29
10.	Same as Figure 9, except that band-to-band recombination effects are included .....	29
11.	Effective lifetime found by simulation as a function of the maximum minority carrier concentration in the sample, for minority carrier lifetimes of 5 nsec, 50 nsec, and 100 nsec .....	32
12.	Band-to-band, Shockley-Read-Hall, and Auger recombination rates as a function of the maximum minority carrier density in the sample, for three different minority carrier lifetimes of 5 nsec, 50 nsec, and 100 nsec .....	35
13.	Band-to-band, Shockley-Read-Hall, and Auger effective lifetimes as a function of the maximum minority carrier density in the sample, for three different minority carrier lifetimes of 5 nsec, 50 nsec, and 100 nsec .....	37
14.	Same as Figure 11, except that equilibrium carrier concentration in sample is $1 \times 10^{14}$ instead of $2 \times 10^{17} \text{ cm}^{-3}$ .....	37
15.	Same as Figure 12, except that equilibrium carrier concentration in sample is $1 \times 10^{14}$ instead of $2 \times 10^{17} \text{ cm}^{-3}$ .....	38

## FIGURES (continued)

16.	Same as Figure 13, except that equilibrium carrier concentration in sample is $1 \times 10^{14}$ instead of $2 \times 10^{17} \text{ cm}^{-3}$ .....	38
17.	Same as Figure 11, except that minority carrier lifetime is kept fixed at 5 nsec and majority carrier lifetime is varied as shown: (a) $N_D = 2 \times 10^{17} \text{ cm}^{-3}$ and (b) $N_D = 1 \times 10^{14} \text{ cm}^{-3}$ .....	39

## TABLE

1.	Parameters Used in the Numerical Solution .....	18
----	---	----

## I. INTRODUCTION

GaAs and AlGaAs alloys are the principal semiconductors used in the production of advanced solar cells. The efficiency of these advanced solar cells is determined primarily by carrier recombination dynamics. A time-correlated single-photon counting technique,<sup>1</sup> commonly referred to as transient photoluminescence (TPL), has become the primary experimental method for the evaluation of minority carrier lifetimes of III-V materials. The TPL method consists of using a pulsed laser to excite carriers in a semiconductor sample, and then monitoring the decay kinetics of the photoluminescence arising from the carrier recombination. Until recently, the minority carrier lifetime properties of these materials were reported as a single lifetime obtained from a TPL measurement.<sup>2</sup> This lifetime was extracted from the photoluminescence decay curve by selecting a region which showed single exponential decay behavior and determining the slope in that region. Thus, the minority carrier lifetime was simply the time required for the measured response curve to fall to  $1/e$  of the value at which the single exponential behavior began. It was assumed that the effects of nonlinear band-to-band (BB) recombination could be avoided through this procedure. However, there was significant scatter in data taken from systematic TPL studies, and the reported minority carrier lifetime values were not always consistent with the performance obtained from solar cells fabricated using the measured material. A recent report<sup>3</sup> on a series of TPL measurements on GaAs and AlGaAs samples showed that the variation in measured lifetimes can arise from the use of different laser excitation intensities in the TPL apparatus.

A typical TPL decay curve for double heterostructure (DH) semiconductor materials is shown plotted in a semi-logarithmic chart in Fig. 1. There are three time domains of importance in the analysis of this result. In the first time domain, TD1, the TPL result shown displays a rapid rise, as carriers are generated in the sample by absorption of the ultrashort optical pulse, followed by a rapid nonlinear decay of the luminescence within a few nanoseconds. The second time domain, TD2, from approximately 25 nsec to 100 nsec, shows luminescence that decays with what appears to be a constant lifetime. Finally, in the third time domain, TD3, the period after 100 nsec, the luminescence decay appears to be the result of a faster process as the signal tails off into the noise. Notice that we can follow this signal over about four orders of magnitude. This is not atypical for these kind of TPL measurements. This particular result was obtained by picosecond optical excitation of a GaAs



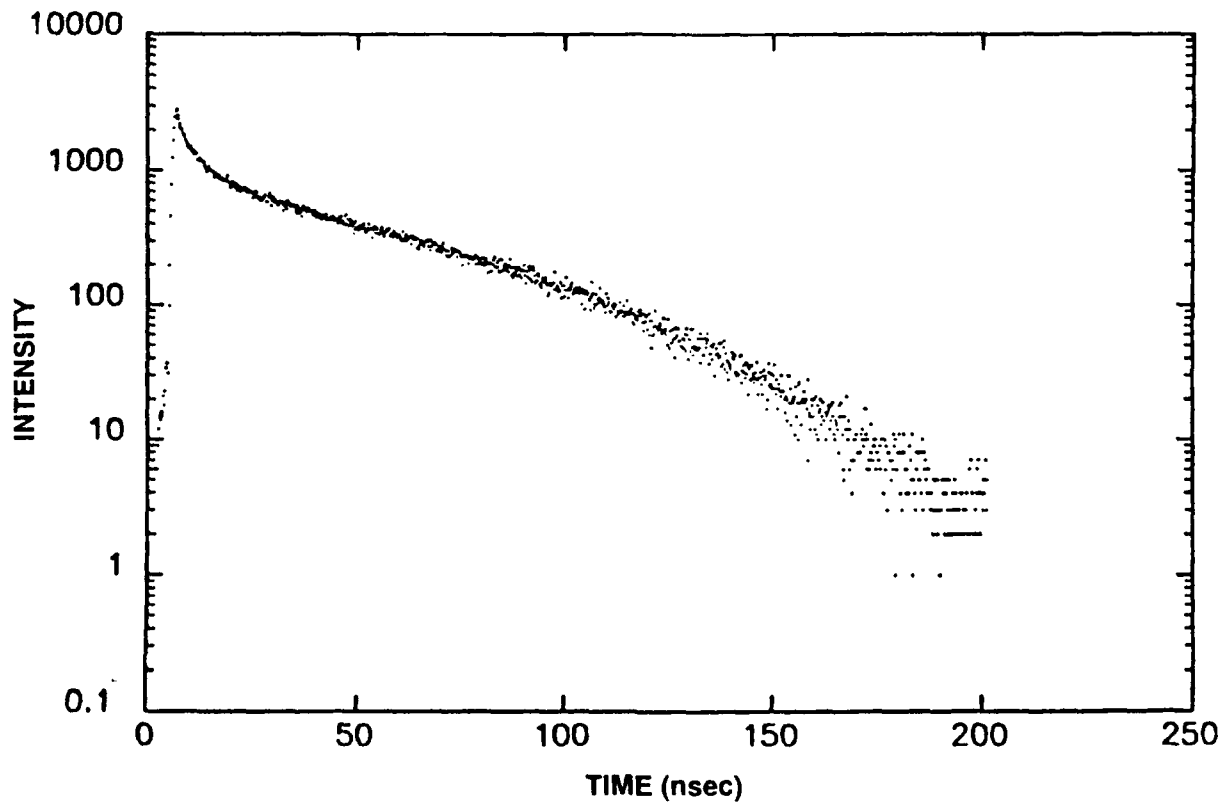


Figure 1. Typical transient photoluminescence decay curve of a GaAs double heterostructure showing emission intensity, in counts, as a function of time.

DH with a train of 20 psec (FWHM of Intensity) optical pulses from a cavity-dumped dye laser with a repetition rate of 400 kHz. The laser wavelength was 590 nm. The average power incident upon the sample was 3.7 mW, and the laser spot was focussed to 82  $\mu\text{m}$  (HW 1/e of Intensity). Consequently, the energy per pulse was 9.25 nJ, and the peak fluence at the sample surface was 0.044 mJ/cm<sup>2</sup>. The GaAs layer was 7  $\mu\text{m}$  thick, sandwiched between two layers of Al<sub>0.9</sub>Ga<sub>0.1</sub>As, each 50 nm thick, all on a GaAs substrate. The temporal resolution of these TPL measurements was approximately 100 psec.

The physical phenomena responsible for the shape of the TPL curve are quite complicated. Excess carriers are injected into the GaAs layers by absorption of the picosecond light pulse. The 590 nm light is strongly absorbed in the GaAs layer. However, the energy bandgap of the Al<sub>0.9</sub>Ga<sub>0.1</sub>As layers is larger than the energy of the quanta, so that little light is absorbed in these layers unless the optical pulse intensity is large enough that two-photon absorption becomes significant. At the optical intensities discussed here, two-photon absorption is negligible in these Al<sub>0.9</sub>Ga<sub>0.1</sub>As layers. The highly nonequilibrium electron-hole plasma thus produced in the GaAs layer evolves rapidly through carrier diffusion, interface recombination, and bulk recombination processes. Part of the bulk recombination is radiative and depends strongly upon the excess carrier concentration. The features of the TPL curve are caused by the changing excess carrier concentration in the sample during this process. At high excess carrier densities ( $\Delta p \gg N_D$ , where  $\Delta p$  is the excess hole concentration and  $N_D$  is the donor density), nonlinear recombination processes such as BB radiative and Auger recombination dominate over processes such as Shockley-Read-Hall (SRH) recombination. These nonlinear processes rapidly reduce the excess carrier concentration, causing the sharp drop observed in the initial signal shown in Fig. 1. At longer times, the excess carrier density is reduced enough that SRH processes can compete with processes such as BB radiative recombination and Auger recombination. Moreover, high excess carrier densities can saturate the SRH recombination centers in the sample and alter the contribution of this process to the effective lifetime. At intermediate carrier densities ( $\Delta p \approx N_D$ ), this saturation of the SRH process can cause the effective lifetime to be dominated by BB recombination, even when the BB lifetime is longer than the minority carrier lifetime. When these effects occur, the lifetime, measured from a single exponential region of the decay curve, is not the true minority carrier lifetime. In fact, it is not clear where on Fig. 1 the slope of the decay curve should be taken

or even if a lifetime extracted from any region of such a curve corresponds to the true minority carrier lifetime. The theory which explains the effects of saturation of the SRH recombination centers was summarized by Blakemore.<sup>4</sup>

Recent observations of the variation of lifetime with excitation intensity were shown to be consistent with SRH theory.<sup>3</sup> Results of TPL measurements on an AlGaAs single heterostructure (SH) at four different excitation intensities are shown in Fig. 2. These results show the decay through regions TD1 and TD2. The transition from region TD2 to region TD3 is not clear in these measurements, probably because of the short lifetimes observed in this sample. The sample was a SH with an approximately 5  $\mu\text{m}$  thick active region of  $n\text{-Al}_{0.38}\text{Ga}_{0.62}\text{As}$  doped at  $N_D = 2 \times 10^{17} \text{ cm}^{-3}$ . The active layer was bounded on the top side by a 100 nm thick layer of  $\text{Al}_{0.8}\text{Ga}_{0.2}\text{As}$ . Lifetimes were extracted from region TD2 using the slope extraction technique described above. The extracted lifetimes for the four measurements of Fig. 2, as well as those of other excitation levels, are shown in Fig. 3 as a function of the excitation level. The carrier densities indicated along the ordinate of Fig. 3 are those peak carrier densities that would occur in the absence of diffusion and recombination, not the actual carrier densities during TD2, from which the lifetime was extracted. The actual carrier densities in region TD2 cannot be determined directly from the TPL measurements. However, over this range of excitation intensities, it is clear that the extracted lifetime is short at low excitation intensities, increases with increasing excitation level, and saturates at a higher value. This, again, is consistent with the saturation of the SRH recombination process described above. Similar measurements on two other AlGaAs SH samples, with doping densities of  $6 \times 10^{16}$  and  $7 \times 10^{16} \text{ cm}^{-3}$ , yielded similar results. The analysis performed previously on these results ignored the effects of BB recombination. As we shall show below, while this analysis was adequate for the results of Fig. 2, the analysis for the other two samples should have included BB recombination effects.

The purpose of this report is to expose the limits of applicability of various simulation techniques from which minority carrier lifetimes have traditionally been extracted. We show that, contrary to recent reports,<sup>2</sup> it is not possible, in general, to extract the true minority carrier lifetime from a single TPL measurement at a selected intensity. We also show that, in general, an intensity study is required to obtain the true recombination properties of a sample. The purpose of this discussion is not to make detailed comparisons of calculated TPL curves

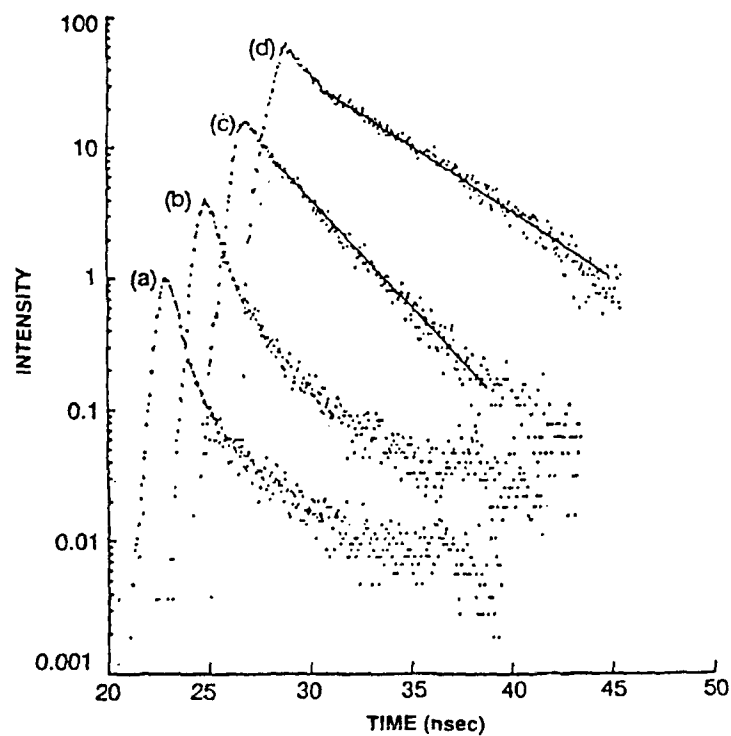


Figure 2. Transient photoluminescence decay measurements at excitation intensities increasing from (a) to (d).

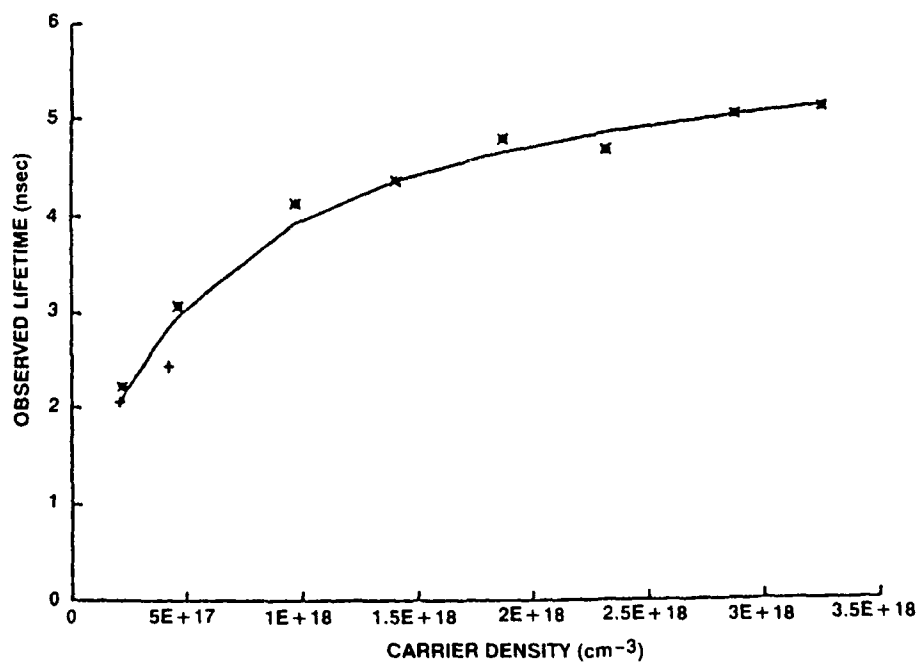


Figure 3. Lifetime extracted from TD2 of the measurements in Figure 2.

with those obtained from measurement. Given that the observed relaxation lifetime depends on the intensity used in the TPL measurement, or equivalently, the instantaneous carrier concentration, there are additional effects which must be considered. In this report, we also investigate the effect of carrier excitation and diffusion characteristics on the TPL method. A more extensive report including comparison with experimental results will be published elsewhere.

## II. SIMULATION METHODS

In the following discussion, we consider the analysis of TPL data using various methods, including: (a) a one-dimensional computer simulation of excess carrier generation, diffusion, and recombination; (b) a recently proposed model<sup>5</sup> that includes only recombination effects but purports to extract both the minority carrier and majority carrier lifetimes; and (c) various other efforts at recombination rate analysis.<sup>6-25</sup> We compare the capabilities and limitations of these methods.

### A. One-dimensional computer simulation

The TPL phenomena we discuss here occur within a three-dimensional spatial volume of a sample photo-excited by an optical pulse with a Gaussian spatial and temporal profile. A complete solution of the complex dynamics involved in the TPL process would involve solving the equations governing the evolution of the photo-excited carriers within the excited volume, including carrier generation, diffusion, and recombination. No known analytical solution exists for this complicated, nonlinear problem. A complete solution can be obtained numerically via a finite-difference approach with two spatial dimensions (one longitudinal and one radial) and the temporal dimension. Such a solution is extremely computationally intensive. However, we can obtain useful insight into the processes involved in TPL with a simpler approach which is less computationally intensive. In this approach, we ignore the radial dimension and solve the problem numerically using a finite difference approach considering one spatial dimension and the temporal dimension.

In order to analyze the full range of carrier dynamic effects on the TPL technique, a time dependent, one-dimensional computer simulation was utilized. As formulated in this section, the solution is explicitly for n-type samples, but similar equations apply for p-type samples. The equation solved is given by

$$dp/dt = G - R_{BB} - R_{SRH} + \nabla \cdot J_D \quad (1)$$

The simulator included models for the following processes: (i) sample excitation by a laser pulse with Gaussian time profile and Beer's law absorption in the semiconductor; (ii) one dimensional, ambipolar diffusion of photogenerated carriers in the sample; (iii) independent front and rear interface recombination velocities; (iv) BB radiative recombination; and (v) nonradiative SRH recombination. The analytic expressions for each of these processes, along with baseline values for the parameters appropriate to GaAs, are given below.

The generation function  $G$  describes the optical generation of excess carriers due to absorption of laser light by the GaAs,

$$G(x,t) = G_0 \exp(-\alpha x) \exp -(t/t_p)^2 \quad (2)$$

with the specified absorption coefficient  $\alpha$ , and pulse width  $t_p$  ( $t_p = 10$  ps), where  $G_0$  takes into account the pulse energy, the spot size on the sample, and the amount of light transmitted into the optically excited region. Carrier diffusion in the sample along the surface normal is accounted for by the standard expression

$$\nabla \cdot J_D = D d^2 p / dx^2 \quad (3)$$

where  $D$  is the ambipolar diffusion coefficient. Interface recombination at the front interface ( $x=0$ ) is described by

$$D dp/dx(x=0) = S_f p(x=0) \quad (4)$$

where  $S_f$  is the front interface recombination velocity. Rear interface ( $x=L$ ) recombination is described by

$$D dp/dx(x=L) = -S_b p(x=L) \quad (5)$$

where  $S_b$  is the rear interface recombination velocity. The BB recombination rate is defined as

$$R_{BB} = B (p n - n_i^2) \quad (6)$$

where  $B$  is the radiative recombination coefficient and  $n_i$  is the intrinsic carrier density. SRH recombination is described by

$$R_{\text{SRH}} = (p N_D + \Delta p^2) / [\tau_p (N_D + \Delta p) + \tau_n \Delta p] \quad (7)$$

where  $\tau_n$  and  $\tau_p$  are the majority and minority carrier lifetimes, respectively.

The primary features of the carrier relaxation process are determined by processes (iv) and/or (v), given by Eqs. (6) and (7). The BB recombination is quadratic in the excess carrier concentrations  $\Delta p = p - p_0$  and  $\Delta n = n - n_0$  (where  $n_0 p_0 = n_i^2$ ) when the excitation, described by the function  $G$ , is large enough that  $\Delta p \gg N_D$ . In this regime, the instantaneous lifetime will vary continuously, and semilog plots of the photoluminescence intensity vs. time will be curved. It will not be apparent where the slope of the decay should be taken to represent the sample lifetime. When  $\Delta p \ll N_D$ , the BB relaxation is pseudo-first order in  $\Delta p$ , i. e.,

$$R_{\text{BB}} = B N_D \Delta p, \quad (8a)$$

and a unique BB lifetime can be defined. For example, the BB lifetime is

$$\tau_{\text{BB}} = 1 / N_D B = 50 \text{ ns} \quad (8b)$$

for  $N_D = 1 \times 10^{17} \text{ cm}^{-3}$  and where  $B = 2 \times 10^{-10} \text{ cm}^3/\text{sec}$ . If BB is the only recombination mechanism, then this will be the observed lifetime. In the majority of samples examined experimentally, SRH recombination is also important. The SRH recombination also shows limiting behavior at high and low excitation. This analysis of SRH recombination is based upon the simple energy level diagram shown in Fig. 4, where the SRH recombination is mediated through a single recombination level located somewhere within the forbidden gap. At high excitation, where  $\Delta p \gg N_D$ , the recombination centers are occupied by electrons and holes, so that the SRH recombination process includes both the capture of holes and electrons. Thus, the SRH rate is



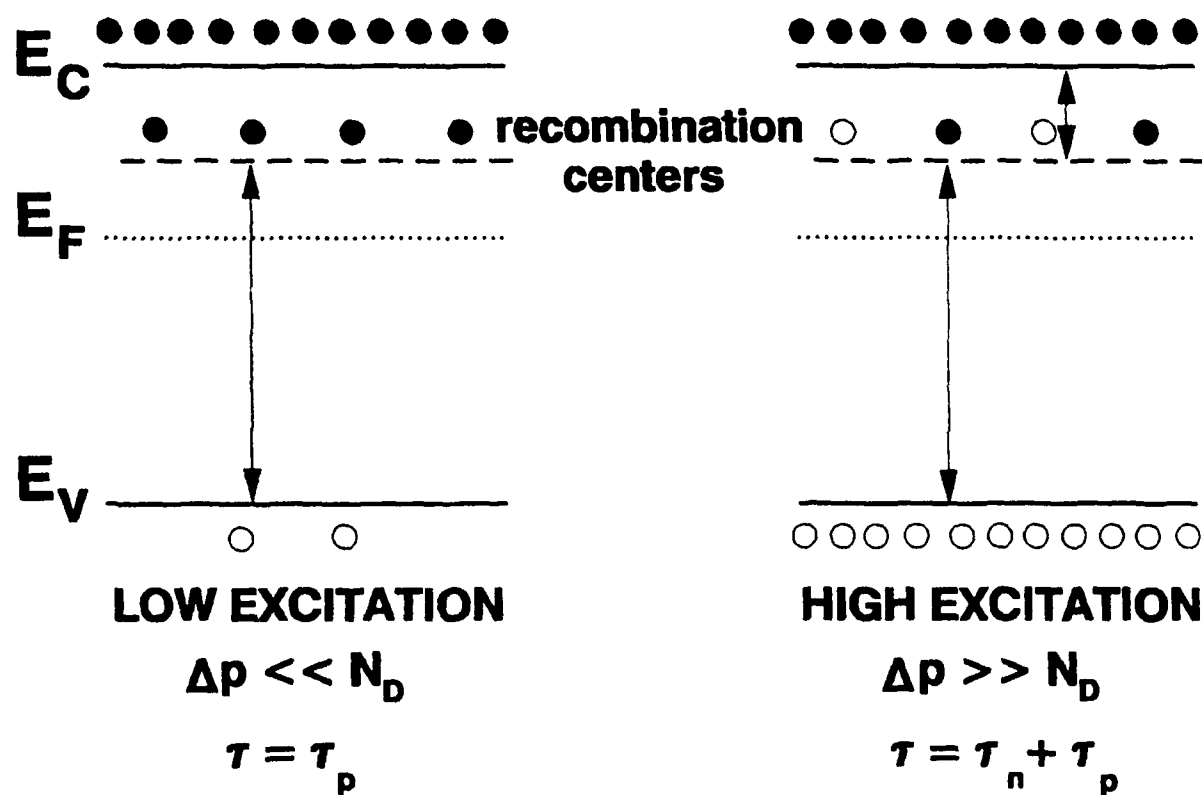


Figure 4. Energy level diagram for the Shockley-Read-Hall recombination process at different limiting excitation intensities.

$$R_{SRH} = \Delta p / (\tau_n + \tau_p), \quad (9)$$

and the effective lifetime due to the SRH process is  $(\tau_n + \tau_p)$ . In the low excitation limit, where  $\Delta p \ll N_D$ , the recombination centers are occupied predominantly by electrons, so that the SRH process is dominated by the capture of holes, and the SRH rate is

$$R_{SRH} = \Delta p / \tau_p \quad (10)$$

so that the effective lifetime due to the SRH process is  $\tau_p$ . Note that the significance of the inequality  $\Delta p \ll N_D$  that was used to obtain Eq.(10) from Eq.(7) depends upon the relationship between the minority carrier and majority carrier lifetimes. If  $\tau_n \cong \tau_p$ , then the low excitation regime can be reached at carrier densities up to about 10% of  $N_D$ . If  $\tau_n \cong 10 \tau_p$ , then the low excitation regime can be reached at carrier densities up to about 1% of  $N_D$ . If  $\tau_n \cong 100 \tau_p$ , then the low excitation regime can be reached at carrier densities up to about 0.1% of  $N_D$ . Thus, the interplay between the BB and SRH processes can be expected to produce a number of lifetime variations with excitation intensity and time. This interplay depends critically upon the relationship between  $\tau_n$ ,  $\tau_p$ , and  $N_D$ . One of the primary purposes of this work is to explore the range of these effects with a minimal number of approximations.

Internal electric fields are not treated in (i)-(v), in order to simplify the convergence of the simulation. This approximation is reasonable when there are no junctions present, and only ambipolar diffusion and recombination occur. Inherent in this approximation is the inability to treat the effect of band bending at interfaces on carrier transport. Auger recombination was also not included in this simulation. However, its absence will not affect the conclusions drawn from this analysis. We also do not include the effects of photon recycling<sup>5</sup> in this analysis.

Various kinds of DHs were studied. The DHs consisted of active regions of either GaAs or AlGaAs, with confinement layers of  $Al_{0.9}Ga_{0.1}As$ . Two different thicknesses of AlGaAs samples are treated. The values used for the parameters in the above equations are listed in Table 1. The values chosen for the majority and minority carrier lifetimes are

$\tau_n = 50$  nsec and  $\tau_p = 5$  nsec. These lifetime values are reasonable for good quality GaAs and  $\text{Al}_x\text{Ga}_{1-x}\text{As}$ . The values for the ambipolar diffusion coefficient were calculated from mobility values for both electrons and holes,<sup>26</sup> using the Einstein relation to convert mobilities to diffusion coefficients and then using  $D = 2D_n D_p / (D_n + D_p)$ . The values for absorption coefficient were obtained from the Handbook of Optical Constants of Solids.<sup>27,28</sup> The radiative recombination coefficient  $B$  was chosen to have the value commonly cited in the literature.<sup>2,5,10,11,21</sup> Some reports have recently suggested that this value may vary slightly with doping level.<sup>6,9</sup> This is unlikely.<sup>29</sup> However, even if true, such a variation would not alter the conclusions stated herein.

Figure 5 shows the temporal dependence of the BB recombination rate computed using Eqs. (1)-(7) for a GaAs DH under several excitation intensities. TPL measurements represent the amount of light collected from the entire excitation volume during each time interval. The results shown in Fig. 5 were calculated at each point in time by evaluating the radiative rate,

TABLE 1. Parameters Used in the Numerical Solution.

SAMPLES	GaAs	$\text{Al}_{0.32}\text{Ga}_{0.68}\text{As}$		$\text{Al}_{0.08}\text{Ga}_{0.92}\text{As}$	
L ( $\mu\text{m}$ )	5	5	15	5	15
$\alpha$ ( $\text{cm}^{-1}$ )	$5.11 \times 10^4$	$3.56 \times 10^4$	$3.56 \times 10^4$	$4.24 \times 10^4$	$4.24 \times 10^4$
$t_p$ (psec)	10	10	10	10	10
D ( $\text{cm}^2/\text{sec}$ )	19.2	9.8	9.8	16.7	16.7
$S_f$ (cm/sec)	1000	1000	1000	1000	1000
$S_b$ (cm/sec)	1000	1000	1000	1000	1000
B ( $\text{cm}^3/\text{sec}$ )	$2 \times 10^{10}$	$2 \times 10^{10}$	$2 \times 10^{10}$	$2 \times 10^{10}$	$2 \times 10^{10}$
$n_i$ ( $\text{cm}^{-3}$ )	$1 \times 10^6$	$1 \times 10^6$	$1 \times 10^6$	$1 \times 10^6$	$1 \times 10^6$
$\tau_n$ (nsec)	50	50	50	50	50
$\tau_p$ (nsec)	5	5	5	5	5

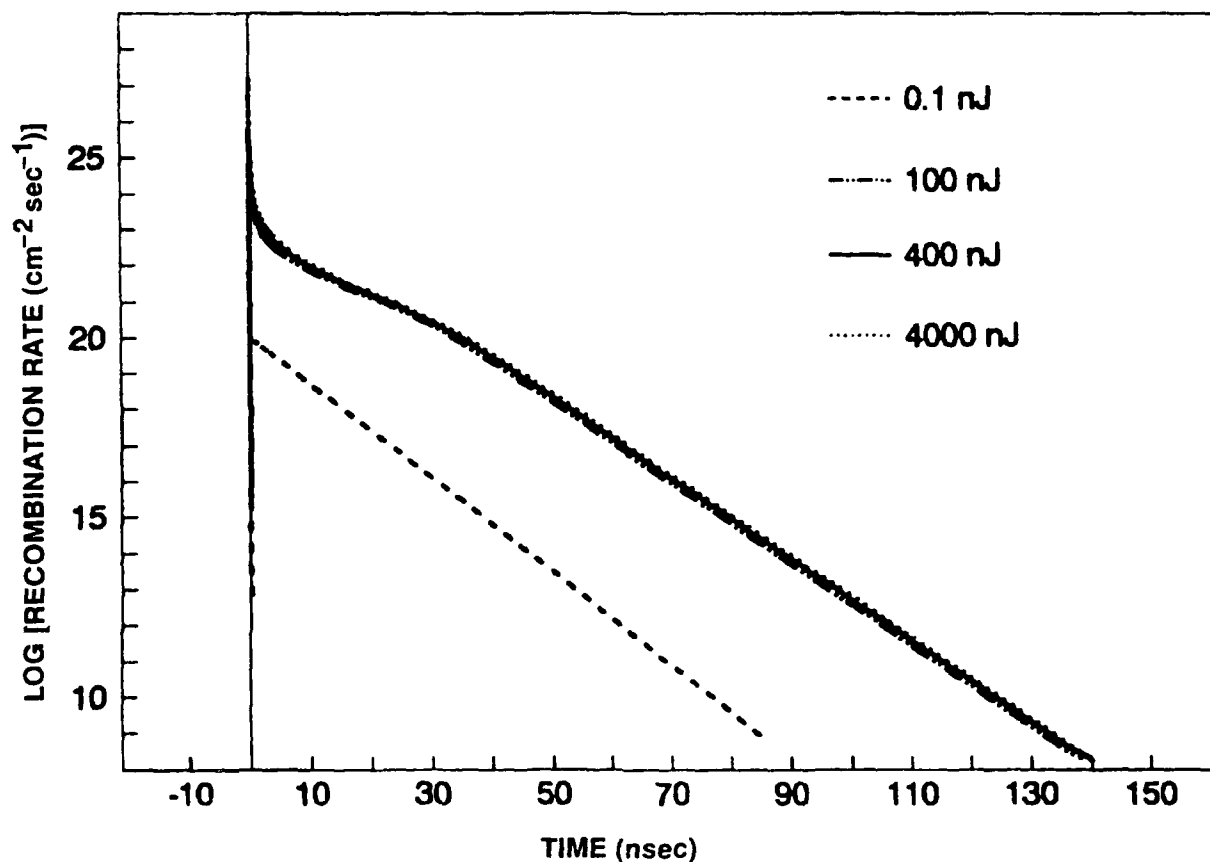


Figure 5. Calculated band-to-band recombination rate, integrated over sample thickness, as function of time for GaAs double heterostructure. This rate is assumed to be proportional to the experimentally observed luminescence intensity at the corresponding time. The curves each represent results from a different assumed laser pulse energy: 0.1 nJ (solid line), 100 nJ (dotted line), 400 nJ (dot-dashed), and 4000 nJ (dashed line).

given by Eq. (6), at every spatial point and integrating the result over the thickness of the sample. This one-dimensionally integrated radiative rate is assumed to represent the signal observed in the TPL experiment, since all other significant recombination mechanisms are nonradiative. Of course, the excess carrier population in the sample at a given time is being determined by both BB and SRH processes. The curves correspond to excitation pulse energies of 0.1, 100, 400, and 4000 nJ. These pulse energies correspond to incident fluences of  $0.00043 \text{ mJ/cm}^2$ ,  $0.430 \text{ mJ/cm}^2$ ,  $1.72 \text{ mJ/cm}^2$ , and  $17.2 \text{ mJ/cm}^2$ , respectively. The carrier concentration of the GaAs before illumination is  $1 \times 10^{17} \text{ cm}^{-3}$  n-type, and the excitation spot is Gaussian with a radius of  $86 \text{ } \mu\text{m}$  (HW 1/e of intensity). The 0.1 nJ simulation shows a single exponential decay with a characteristic time of approximately 5 ns, which corresponds well with  $\tau_p$ . The decay curves at the three higher pulse energies are similar to the result of the TPL measurement shown in Fig. 1, showing qualitatively similar features as the TPL measurement in all three time domains of interest. For these three fluences, TD2 is relatively short, ending at about 40 nsec, followed by single exponential behavior in TD3. These three results are essentially identical during TD2 and TD3. The reason that the shape of the decay curve becomes independent of pulse energy in the high energy limit is due to the effectiveness of the nonlinear BB recombination process. At high excess carrier concentrations, BB recombination dominates and quickly reduces the excess carrier concentrations to levels where the recombination becomes dominated by the other processes described above. Consequently, at high excess carrier concentrations, in the temporal region within a few nanoseconds of excitation, the excess carrier recombination evolves rapidly and is dominated by BB recombination. In the temporal region beyond a few nanoseconds after excitation, there is an effective saturation of the excess carrier concentration. This result is significant because it indicates that there is a limit to the level of excitation which can be achieved experimentally in the time domain of interest, i. e., in the time domain from which carrier lifetimes are usually extracted. Another aspect of this phenomenon is that since the observed decay curve will appear to be independent of excitation level, this might be mistaken for the low excitation limit, unless one examines carefully the response within the first few nanoseconds of excitation.

Inspection of Eq. (9) suggests that for samples in which SRH recombination is important, sufficiently high excitation levels will produce single exponential decays with the

effective lifetime  $(\tau_n + \tau_p)$ . However, under the realistic conditions just simulated, it is clear that the BB process might prevent this situation from being achieved. In particular, depending on the relative magnitudes of the BB coefficient [Eq. (6)] and the carrier lifetimes, it may not be possible to observe a time regime where the decay time is either  $\tau_p$  or  $(\tau_n + \tau_p)$ .

In Fig. 6(a)-6(d), we show results of one-dimensional simulations of 15  $\mu\text{m}$  thick  $\text{Al}_x\text{Ga}_{1-x}\text{As}$  DHs for excitation energies of 0.1, 400, and 4000 nJ. Results are shown for: (a)  $x = 0.32$ ,  $N_D = 2 \times 10^{17} \text{ cm}^{-3}$ ; (b)  $x = 0.32$ ,  $N_D = 2 \times 10^{16} \text{ cm}^{-3}$ ; (c)  $x = 0.08$ ,  $N_D = 2 \times 10^{17} \text{ cm}^{-3}$ ; (d)  $x = 0.08$ ,  $N_D = 2 \times 10^{16} \text{ cm}^{-3}$ . Here, the results are qualitatively similar to those shown for the GaAs DH. The results at 0.1 nJ excitation are all essentially single exponential. Again, as with the results for the GaAs DH, the simulations at the higher excitation energies are virtually identical at times longer than a few nanoseconds. In comparing Fig. 6(a) to Fig. 6(c), we see that there is little difference in the simulations relative to the proportions of Al and Ga in the DH. Similar comparison of Fig. 6(b) to Fig. 6(d) yields the same result. However, in comparing Fig. 6(a) to Fig. 6(b), we see that there are substantial differences in the slopes of the simulations at the longer time delays for samples with the same alloy but different donor densities. Remember that, within this time domain, the BB recombination rate has become pseudo-first order and the BB lifetime has become constant. This constant BB lifetime, from Eq. (9), is 25 nsec for a donor density of  $2 \times 10^{17} \text{ cm}^{-3}$  and is 250 nsec for a donor density of  $2 \times 10^{16} \text{ cm}^{-3}$ . Consequently, if  $\Delta p \ll N_D$ , the effective lifetime is given by

$$1/\tau_{\text{eff}} = 1/\tau_{\text{BB}} + 1/\tau_p, \quad (11)$$

which yields an effective lifetime of 4.17 nsec for the sample doped to  $2 \times 10^{17} \text{ cm}^{-3}$  and an effective lifetime of 4.9 nsec for the samples doped to  $2 \times 10^{16} \text{ cm}^{-3}$ . Even though the curves approach a single exponential response, the slope of the response is not the minority carrier lifetime unless  $\tau_p \ll \tau_{\text{BB}}$ . While this effect does not seem remarkable from the examples given, leading to a 20% difference in one case and a 2% difference from the minority carrier lifetime in the other case, consider the confusion if, for example,  $\tau_p = 100 \text{ nsec}$ . For this value of the minority carrier lifetime, the effective lifetimes would be 20 nsec and 71 nsec for the two doping densities. Simple extraction of the minority carrier lifetime from the slope of a

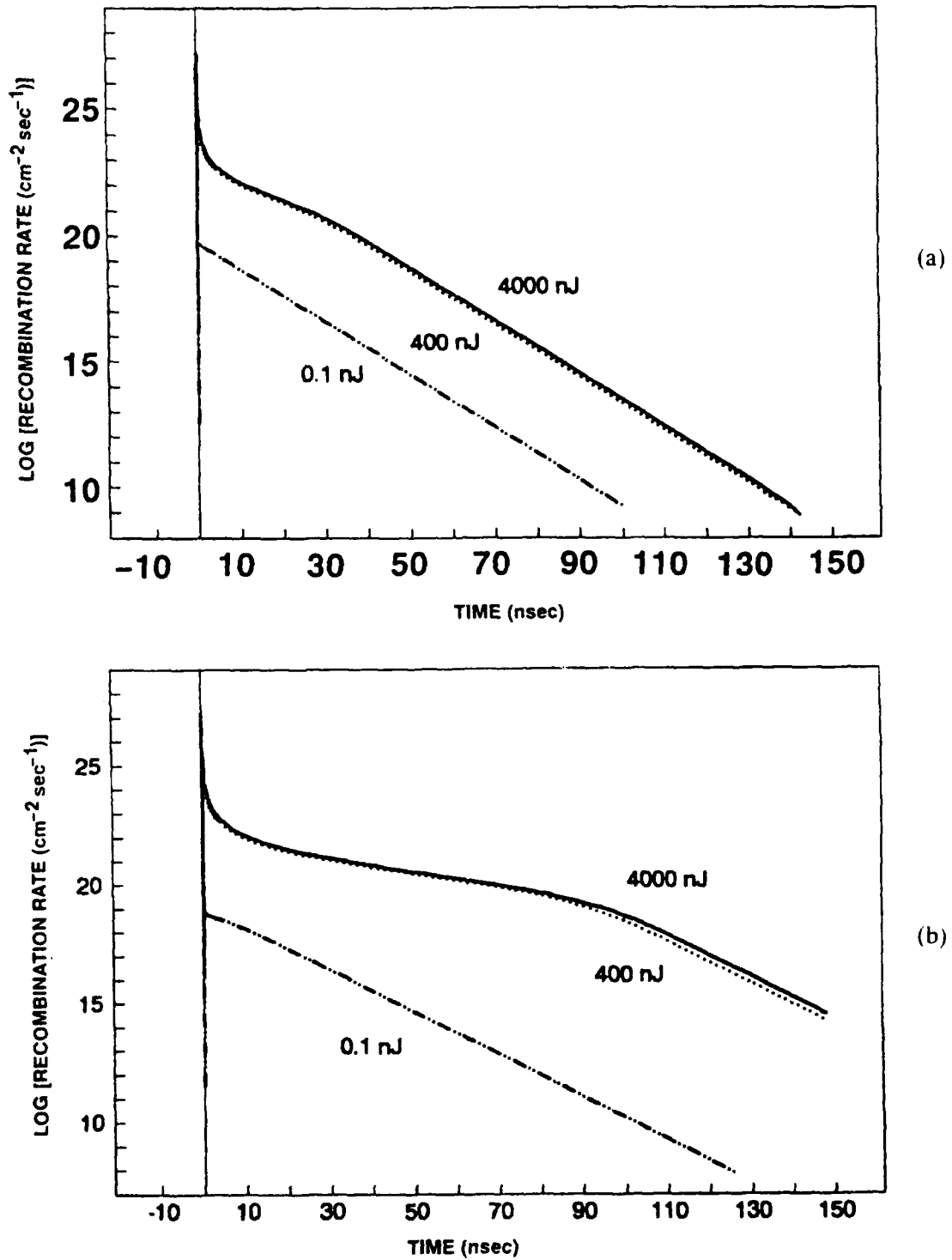


Figure 6. Results of one-dimensional simulations of integrated band-to-band recombination in  $15 \mu\text{m}$  thick  $\text{Al}_x\text{Ga}_{1-x}\text{As}$  double heterostructures for excitation energies of 0.1 nJ (dot-dashed line), 400 nJ, (dotted line), and 4000 nJ (solid line). Results are shown for: (a)  $x = 0.32$ ,  $N_D = 2 \times 10^{17} \text{ cm}^{-3}$ ; (b)  $x = 0.32$ ,  $N_D = 2 \times 10^{16} \text{ cm}^{-3}$ .

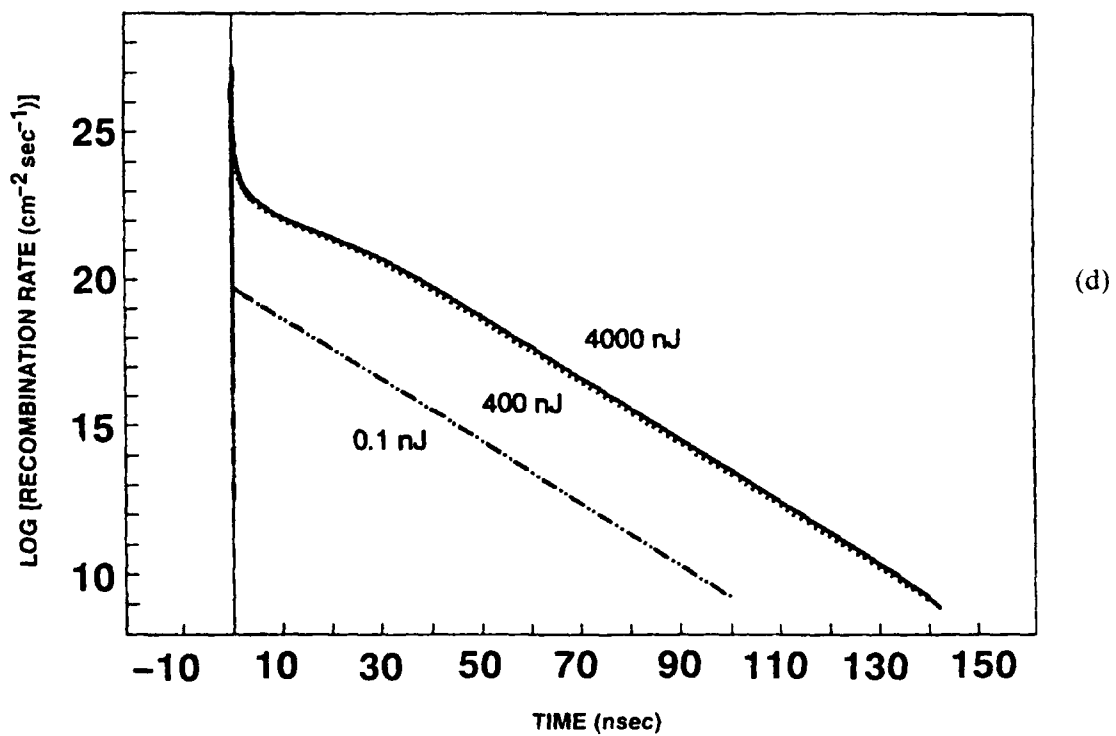
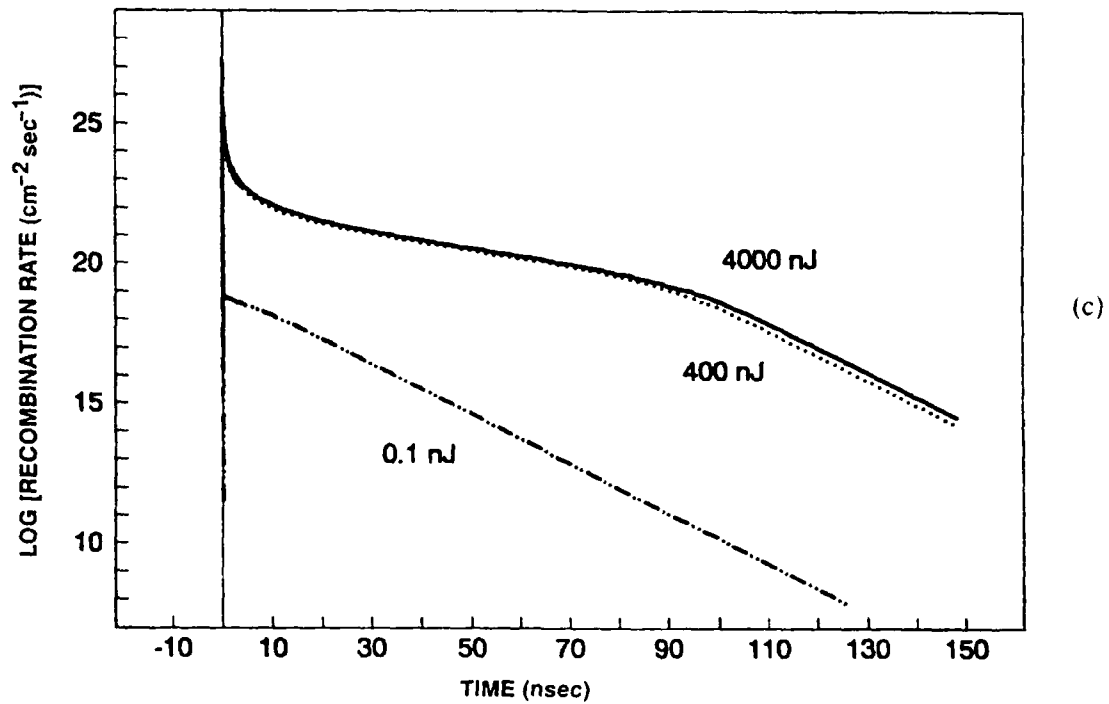


Figure 6. Results of one-dimensional simulations of integrated band-to-band recombination in 15  $\mu\text{m}$  thick  $\text{Al}_x\text{Ga}_{1-x}\text{As}$  double heterostructures for excitation energies of 0.1 nJ (dot-dashed line), 400 nJ, (dotted line), and 4000 nJ (solid line). Results are shown for: (c)  $x = 0.08$ ,  $N_D = 2 \times 10^{17} \text{ cm}^{-3}$ ; (d)  $x = 0.08$ ,  $N_D = 2 \times 10^{16} \text{ cm}^{-3}$ .



measured TPL curve thus requires accurate knowledge of both the donor density and the BB recombination coefficient.

In Fig. 7(a)-7(d), we show results of one-dimensional simulations of thinner, 5  $\mu\text{m}$  thick  $\text{Al}_x\text{Ga}_{1-x}\text{As}$  DHs for excitation energies of 0.1, 400, and 4000 nJ. Results are shown for: (a)  $x = 0.32$ ,  $N_D = 2 \times 10^{17} \text{ cm}^{-3}$ ; (b)  $x = 0.32$ ,  $N_D = 2 \times 10^{16} \text{ cm}^{-3}$ ; (c)  $x = 0.08$ ,  $N_D = 2 \times 10^{17} \text{ cm}^{-3}$ ; (d)  $x = 0.08$ ,  $N_D = 2 \times 10^{16} \text{ cm}^{-3}$ . Here, again, the results are qualitatively similar to those shown for the 15  $\mu\text{m}$  thick AlGaAs DHs. The differences are marginal and are due to the differing effects of diffusion within the DHs on the resulting carrier density. Remember that the carriers are initially deposited near the front interface and diffuse rapidly into the material. Diffusion is more effective in producing a uniform carrier distribution throughout the optically excited region for the thinner structures. The conclusions we draw from this set of simulations are identical to those drawn from the results for the 15  $\mu\text{m}$  thick DHs.

The TPL curves shown in Figs. 5-7 cover a wide span of incident optical pulse energies. In each figure, one result is presented at 0.1 nJ incident energy. The TPL response for this energy is essentially a single exponential response indicating that  $\Delta p \ll N_D$ . The TPL curves at the other energies in the Figs. 5-7 are all at incident optical pulse energies substantially higher than the measured TPL response shown in Fig. 1. However, the phenomena responsible for the formation of TPL curves similar to those shown in Fig. 1 begin to make themselves evident at incident optical energies between 0.1 nJ and 100 nJ. In Fig. 8(a) and 8(b), we show the results of simulations of optical excitation of the 5  $\mu\text{m}$  thick  $\text{Al}_{0.08}\text{Ga}_{0.92}\text{As}$  DH at energies of 0.1, 1, 5, 10, and 50 nJ. In Fig. 8(a),  $N_D = 2 \times 10^{16} \text{ cm}^{-3}$ , whereas in Fig. 8(b),  $N_D = 2 \times 10^{17} \text{ cm}^{-3}$ . The difference between TD2 and TD3 can be clearly distinguished at incident energies as low as 1 nJ for the less heavily doped sample. The corresponding fluence for this spot size would be  $4.3 \mu\text{J}/\text{cm}^2$ . Furthermore, all of the simulated curves at energies greater than 1 nJ show the sharp peak during and immediately after the excitation process that is indicative of the nonlinear BB and SRH recombination processes.

Finally, note that in these simulated TPL curves in Figs. 5-8, we follow the results over many orders of magnitude. In reality, the signal-to-noise limits of the light collection and detection system would impose a floor below which no signal would be observable (see the appendix). The lowest signal levels are observed in TD3, from which one hopes to

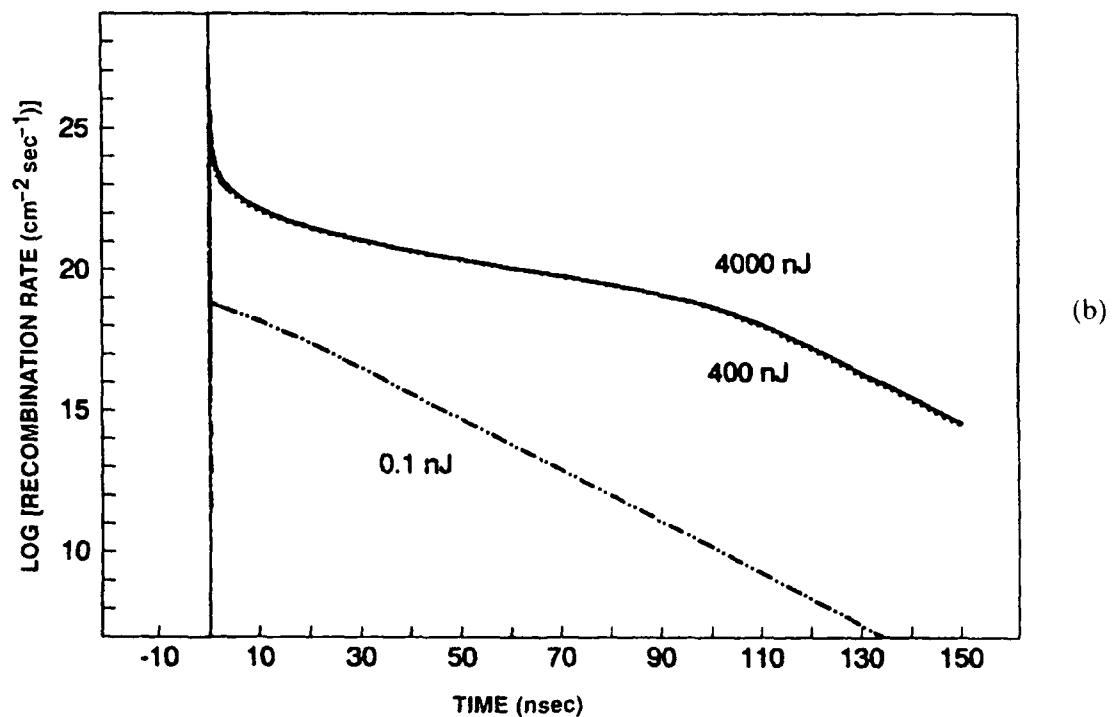
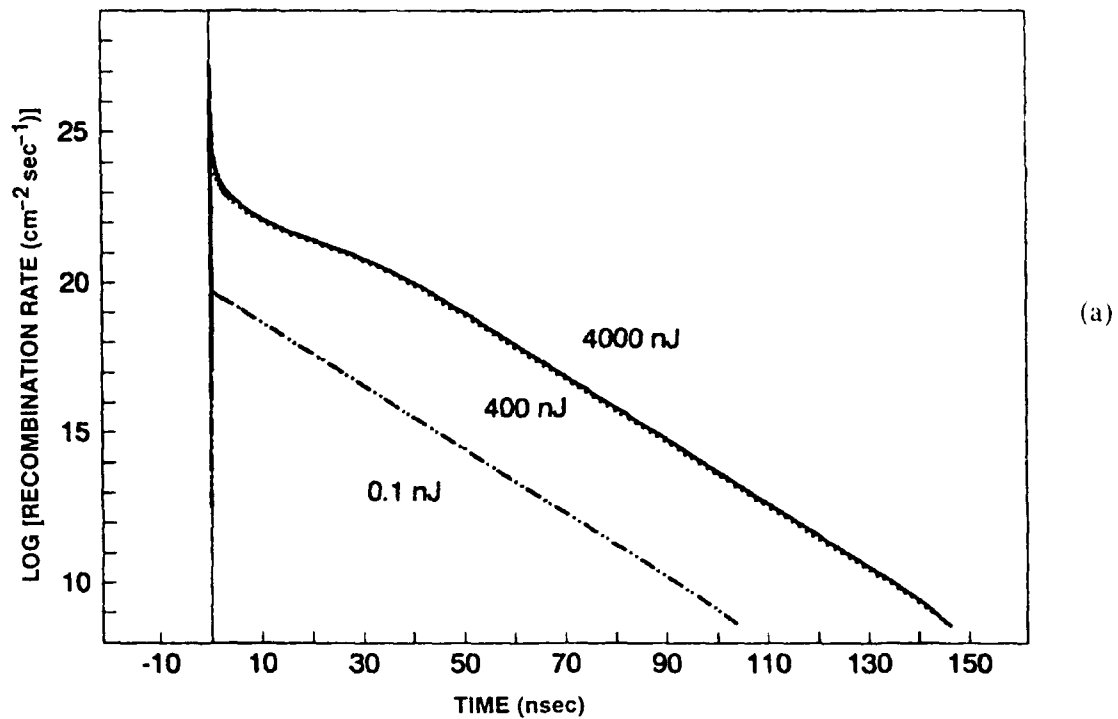


Figure 7. Results of one-dimensional simulations of integrated band-to-band recombination in 5  $\mu\text{m}$  thick  $\text{Al}_x\text{Ga}_{1-x}\text{As}$  double heterostructures for excitation energies of 0.1 nJ (dot-dashed line), 400 nJ, (dotted line), and 4000 nJ (solid line). Results are shown for: (a)  $x = 0.32$ ,  $N_D = 2 \times 10^{17} \text{ cm}^{-3}$ ; (b)  $x = 0.32$ ,  $N_D = 2 \times 10^{16} \text{ cm}^{-3}$ .

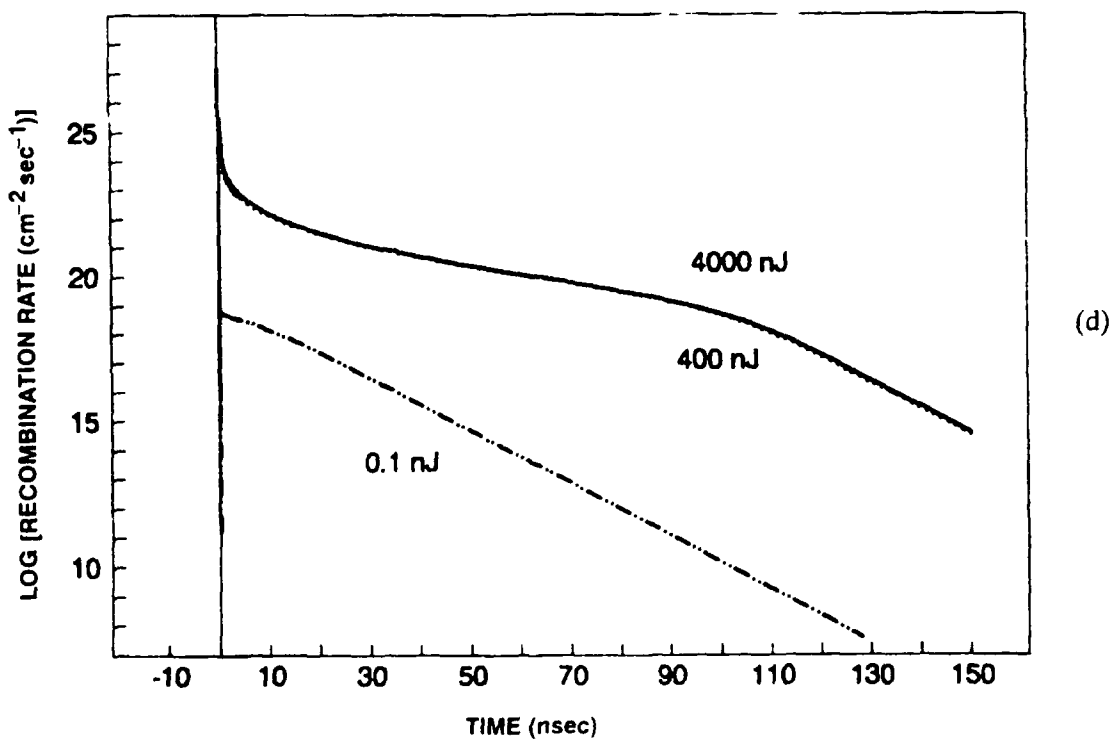
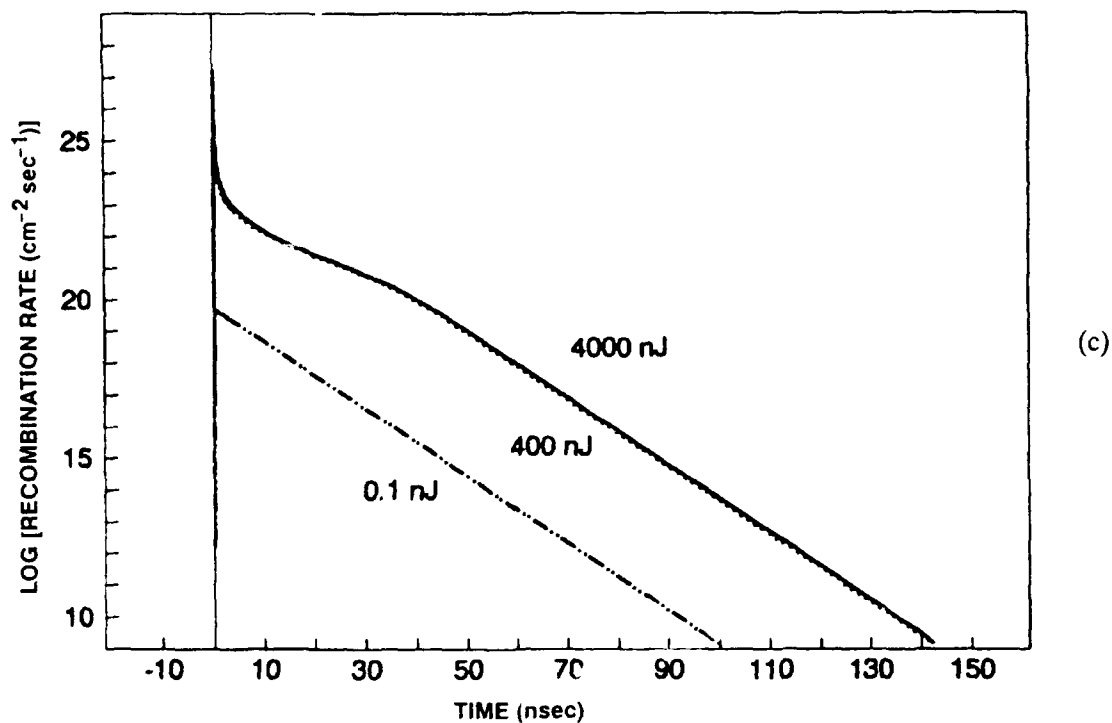


Figure 7. Results of one-dimensional simulations of integrated band-to-band recombination in 5  $\mu\text{m}$  thick  $\text{Al}_x\text{Ga}_{1-x}\text{As}$  double heterostructures for excitation energies of 0.1 nJ (dot-dashed line), 400 nJ, (dotted line), and 4000 nJ (solid line). Results are shown for: (c)  $x = 0.08$ ,  $N_D = 2 \times 10^{17} \text{ cm}^{-3}$ ; (d)  $x = 0.08$ ,  $N_D = 2 \times 10^{16} \text{ cm}^{-3}$ .

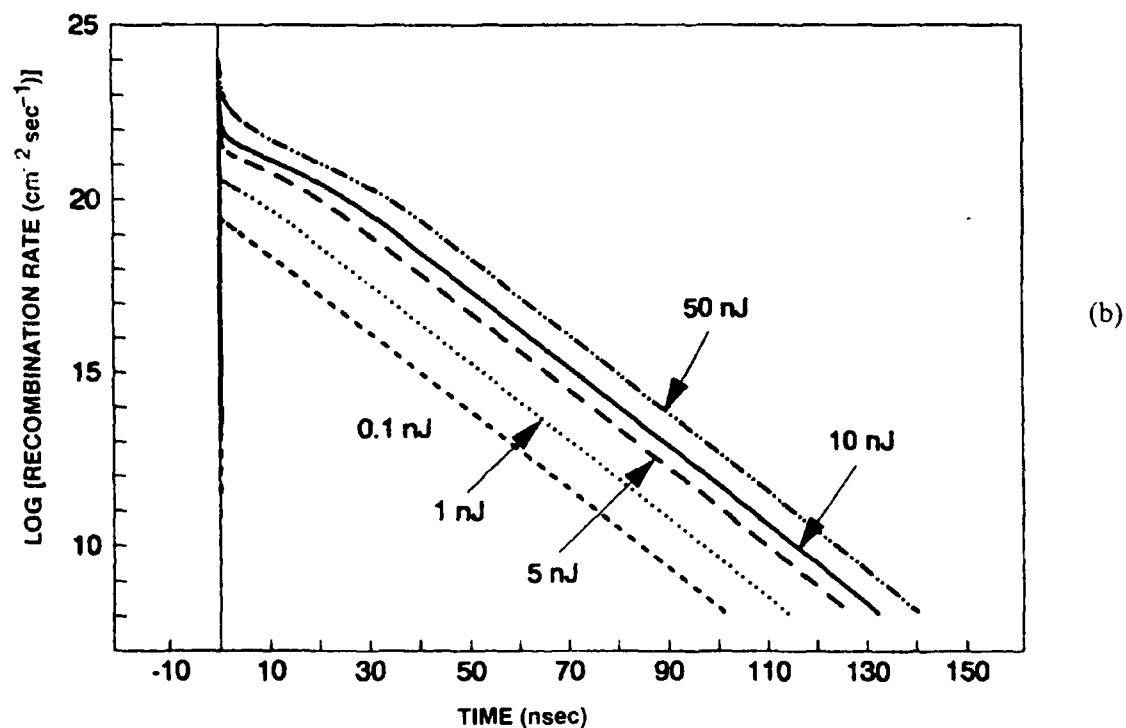
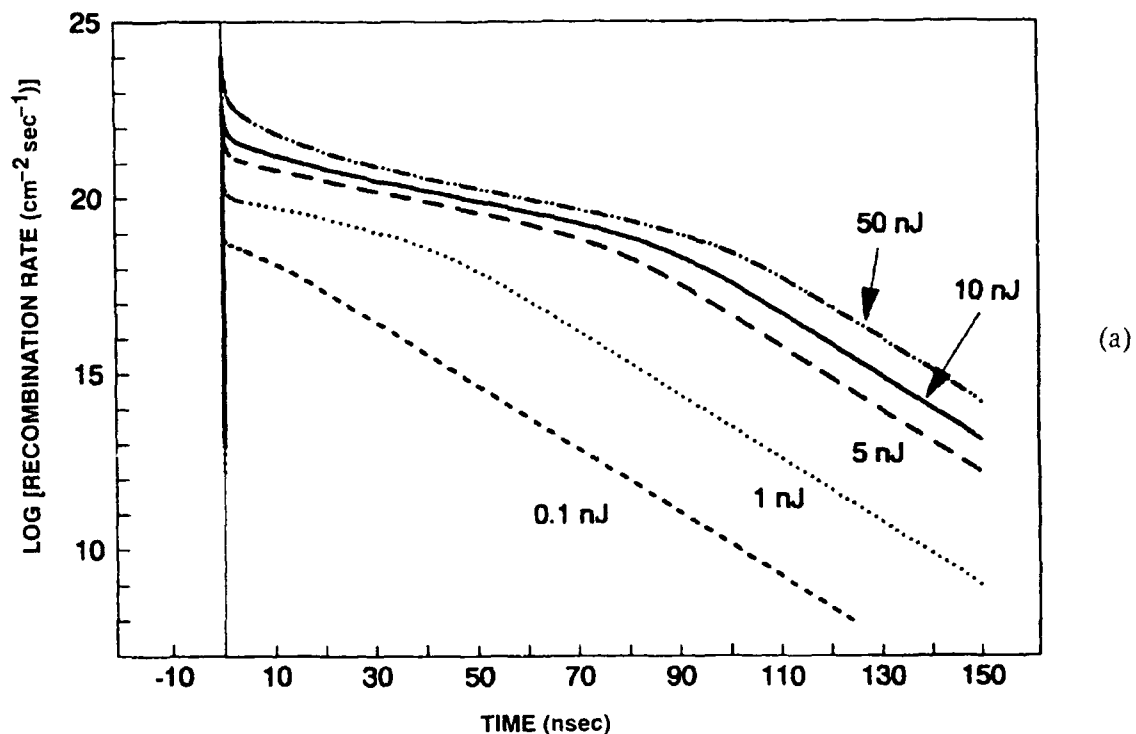


Figure 8. Results of one-dimensional simulations of integrated band-to-band recombination in 5  $\mu\text{m}$  thick  $\text{Al}_{0.08}\text{Ga}_{0.92}\text{As}$  double heterostructures for excitation energies of 0.1 nJ (short-dashed line), 1 nJ, (dotted line), 5 nJ (long-dashed line), and 50 nJ (dot-dashed line). Results are shown for: (a)  $N_D = 2 \times 10^{16} \text{ cm}^{-3}$  and (b)  $N_D = 2 \times 10^{17} \text{ cm}^{-3}$ .

unambiguously extract information concerning the minority carrier lifetime. If observation of the TPL response in this time domain is limited by signal-to-noise considerations, then the extraction of the minority carrier lifetime becomes more problematical. Thus, over the range of thicknesses discussed here (i. e., 5-15  $\mu\text{m}$ ) and over the range of alloy parameters discussed (i.e.,  $x=0.08-0.32$ ), we conclude that extraction of carrier lifetimes from TPL measurements requires extremely careful analysis of the results.

#### B. Recombination effects model

Recently, Ahrenkiel and coworkers have developed a simpler model based upon SRH recombination alone to analyze the results of TPL measurements.<sup>5</sup> They obtain a relatively simple nonlinear differential equation by ignoring the early stages of the excitation/relaxation process and the BB process. In this approximation, a uniform carrier distribution is assumed to develop after a few nanoseconds, and the problem is solved only from that time onward. The initial excess carrier concentration is simply obtained by distributing all of the generated carriers uniformly throughout the sample volume. In this approximation, Eq. (1) is replaced by  $dp/dt = -R_{\text{SRH}}$ , where  $R_{\text{SRH}}$  is defined in Eq. (7). The exact values of the carrier densities are imposed as an initial condition at this point in their analysis. We have solved this equation numerically as a function of initial excitation power to obtain the results shown in Fig. 9 in complete agreement with their results.<sup>5</sup> As in Fig. 5, the abscissa is  $R_{\text{BB}}$ , which is assumed to be the experimental observable, i. e., the photoluminous intensity. The labels on the curves indicate the (homogeneous) excess carrier concentration immediately following laser excitation, normalized to the equilibrium concentration of  $2 \times 10^{17} \text{ cm}^{-3}$ . The highest level corresponds to a pulse energy of 38 nJ in the geometry assumed for the results displayed in Fig. 5. The lifetimes assumed are the same as for Fig. 5, namely 5 ns and 50 ns for minority and majority carriers, respectively. However, the family of curves is valid for any choice of lifetimes with a 10:1 majority/minority carrier lifetime ratio. These solutions suggest that for sufficiently high excitation levels, a two-component decay can be observed. The early stages of the decay show lifetimes which are close to  $\tau_n + \tau_p$ , and the later stages, to  $\tau_p$ . In Fig. 9, the curve corresponding to the highest excitation does have an initial slope near  $\tau_n + \tau_p = 55 \text{ ns}$ , and the later slope is near  $\tau_p = 5 \text{ ns}$ . However, the complete solution of the

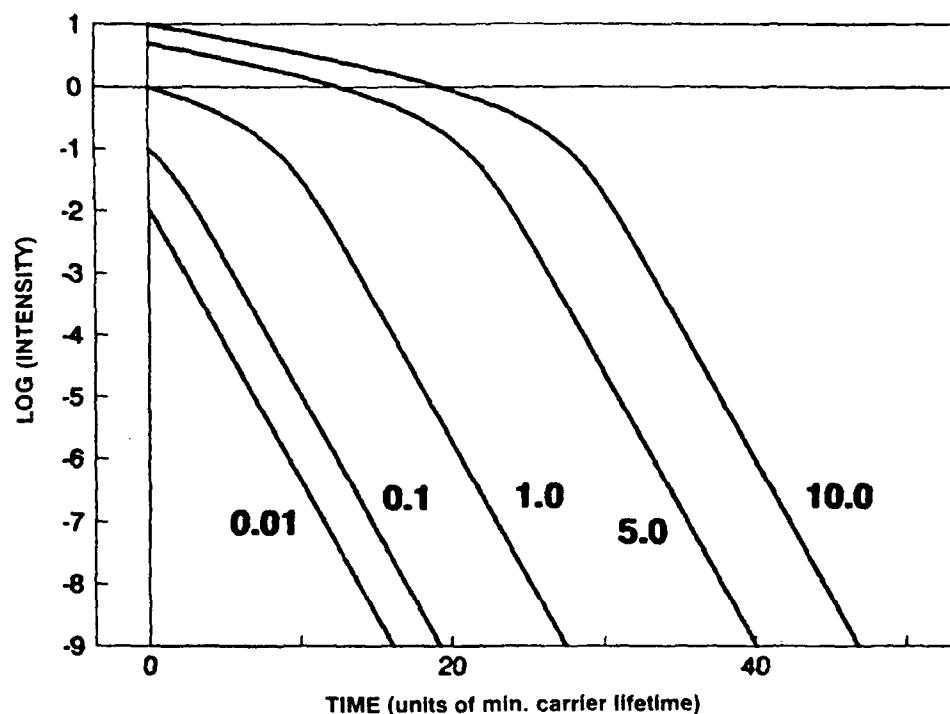


Figure 9. Simulated band-to-band recombination rate in GaAs double heterostructure, assuming uniform distribution of generated carriers and ignoring band-to-band recombination. X-axis represents time, normalized by the minority carrier lifetime. Labels on the curves refer to the excess carrier concentration, normalized by the sample equilibrium carrier density.

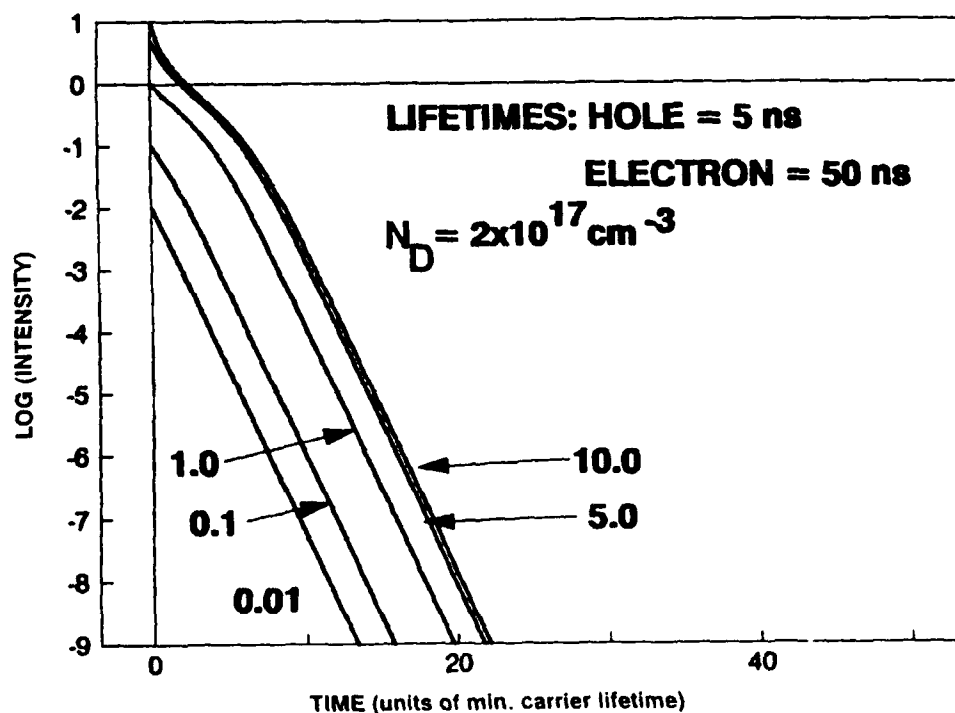


Figure 10. Same as Figure 9, except that band-to-band recombination effects are included.

problem presented in the preceding section shows that the inclusion of the excitation and other relaxation processes (i) completely removes these simple characteristics and (ii) indicates that, in general, no simple single exponential decay regions exist where lifetimes may be accurately extracted from one decay curve.

Figure 10 shows results of the same calculation as displayed in Fig. 9, but with the effect of BB recombination included, assuming  $N_D = 2 \times 10^{17} \text{ cm}^{-3}$ . The long lifetime region at early times has disappeared, and the later slopes, although roughly parallel to one another, now represent a different effective lifetime than in Fig. 9. Clearly, it is not possible, in general, to extract both the majority carrier and minority carrier lifetimes from the slopes of TPL curves using this type of analysis, unless accurate knowledge of other parameters such as the donor density (for n-type samples), the radiative recombination coefficient, the Auger recombination coefficient, and the interface recombination velocities are obtained. Finally, we point out that the analysis displayed in Fig. 9 also ignores the limitations on the achievable carrier densities, clearly displayed in Fig. 5. These limitations are the result of nonlinear recombination during and immediately after the generation process if the photogenerated carrier density becomes large enough. However, in their analysis, only the curves with large "initial" carrier densities display the plateau-like region with the decay time given by  $\tau_n + \tau_p$ .

### C. Recombination rate analysis

Utilizing the slope measurement technique described in the introduction, some authors<sup>2,3,5,6,7,13,19,20,23,24,25</sup> have extracted a recombination rate from TPL curves, and have ascribed this rate to a variety of recombination processes operating simultaneously, e. g.,

$$R_{\text{tot}} = R_{\text{SRH}} + R_{\text{BB}} + R_{\text{Auger}} + R_{\text{surf}} \quad (12)$$

where  $R_{\text{tot}}$  is the total recombination rate,  $R_{\text{SRH}}$  is the SRH recombination rate,  $R_{\text{BB}}$  is the BB recombination rate,  $R_{\text{Auger}}$  is the Auger recombination rate, and  $R_{\text{surf}}$  is the surface recombination rate. Often, at this point, these rates are approximated as an excess carrier density divided by a lifetime, so that  $R_{\text{tot}} = \Delta p / \tau_{\text{tot}}$ ,  $R_{\text{SRH}} = \Delta p / \tau_{\text{SRH}}$ ,  $R_{\text{BB}} = \Delta p / \tau_{\text{BB}}$ ,  $R_{\text{Auger}} = \Delta p / \tau_{\text{Auger}}$ . The surface recombination rate in these studies is usually approximated

in an ad hoc manner as  $R_{\text{surf}} = 2S\Delta p/d$ , where  $S$  is the surface recombination velocity and  $d$  is the thickness of the luminescing material. This analysis leads to the result

$$1/\tau_{\text{tot}} = 1/\tau_{\text{SRH}} + 1/\tau_{\text{BB}} + 1/\tau_{\text{Auger}} + 2S/d. \quad (13)$$

Note that for small enough values of  $S$  or large enough values of  $d$ , the surface recombination part can be ignored. For a  $5 \mu\text{m}$  thick sample and  $S = 1000 \text{ cm/sec}$ , the surface recombination "lifetime" is  $250 \text{ nsec}$ . For  $S = 100 \text{ cm/sec}$  and  $d = 1 \mu\text{m}$ , the surface recombination "lifetime" is  $500 \text{ nsec}$ . However, for  $S = 10^5 \text{ cm/sec}$  and a  $5 \mu\text{m}$  thick sample, the surface recombination "lifetime" is  $2.5 \text{ nsec}$ . Thus, care must be taken when considering the effects of interface recombination. In many cases, the analysis for n-type samples uses

$$\tau_{\text{SRH}} = \tau_p, \quad (14a)$$

$$\tau_{\text{BB}} = 1/BN_D, \quad (14b)$$

and

$$\tau_{\text{Auger}} = 1/CN_D^2, \quad (14c)$$

where  $B$  is the radiative recombination coefficient,  $C$  is the Auger recombination coefficient, and  $N_D$  is the number density of donors. This analysis is adequate as long as  $\Delta p \ll N_D$  and as long as surface recombination effects are not important. Consequently, it may be reasonable to apply such analysis in TD3, but certainly not within TD1 or TD2. Furthermore, uncertainties in the recombination coefficients or donor densities may preclude accurate extraction of the minority carrier lifetime.

Figure 11 shows results of additional simulations designed to explore the possibility of extracting either  $\tau_p$  or  $\tau_n + \tau_p$  from recombination rate analysis, as has been suggested by Ahrenkiel and coworkers.<sup>5</sup> In what follows, we ignore the effects of interface recombination. Instead of displaying the actual PL decay curves as in the previous figure, Fig. 11 shows the effective lifetime which would be derived from the slope of the decay curve as a function of



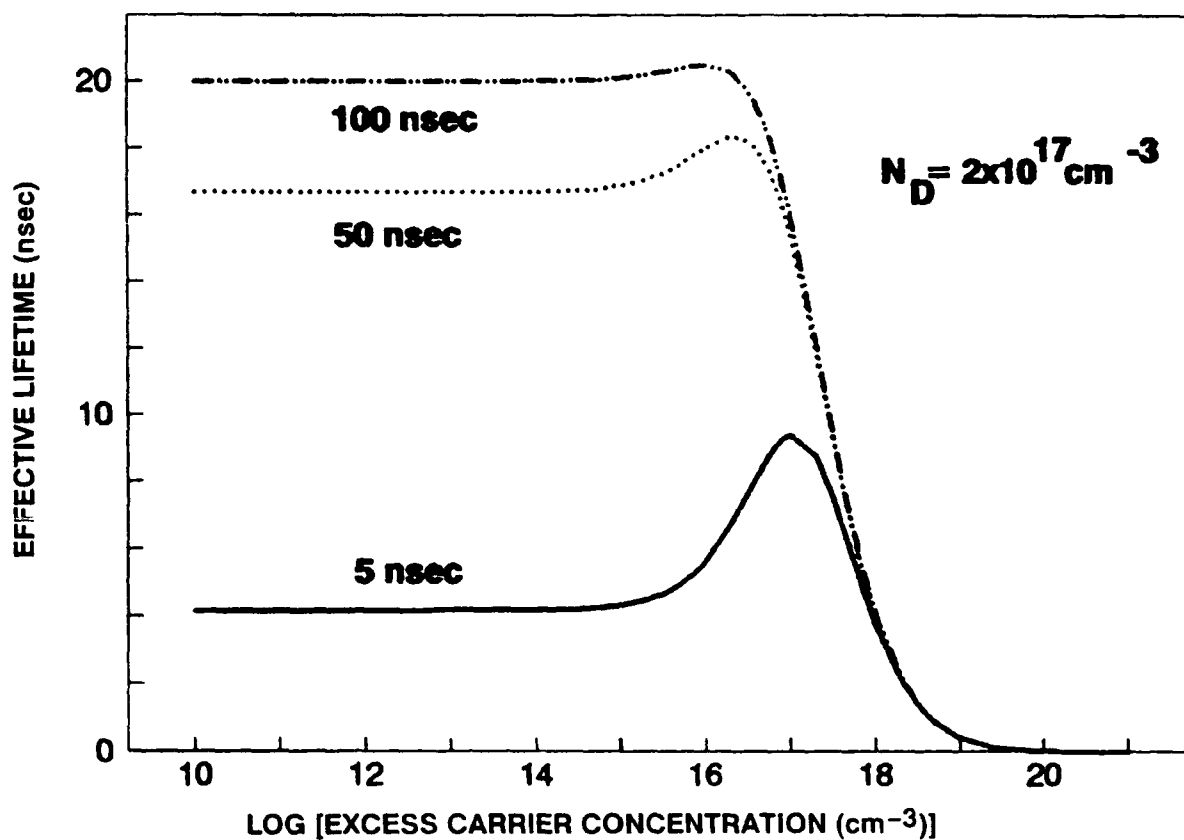


Figure 11. Effective lifetime found by simulation as a function of the maximum minority carrier concentration in the sample, for minority carrier lifetimes of 5 nsec (solid line), 50 nsec (dotted line) and 100 nsec (dot-dashed line). The majority carrier lifetime is ten times the minority carrier lifetime.  $N_D = 2 \times 10^{17} \text{ cm}^{-3}$ .

the maximum value of the excess minority carrier density  $p$  in the sample. These results were obtained by setting the sum of the BB, Auger, and SRH recombination rates equal to  $\Delta p / \tau_{\text{eff}}$  and solving for  $\tau_{\text{eff}}$  as a function of  $\Delta p$ , i.e.,

$$R = R_{\text{SRH}} + R_{\text{BB}} + R_{\text{Auger}} = \Delta p / \tau_{\text{eff}} \quad (15a)$$

or

$$\tau_{\text{eff}} = \Delta p / (R_{\text{SRH}} + R_{\text{BB}} + R_{\text{Auger}}) \quad (15b)$$

where  $R_{\text{SRH}}$  and  $R_{\text{BB}}$  are defined as in Eqs. (6) and (7) above, and  $R_{\text{Auger}}$  is defined as

$$R_{\text{Auger}} = C_p(np^2 - N_D p_0^2) + C_n(pn^2 - p_0 N_D^2) \quad (16)$$

with  $C_p = 4 \times 10^{-30} \text{ cm}^6/\text{sec}$  and  $C_n = 1.8 \times 10^{-31} \text{ cm}^6/\text{sec}$ ,<sup>30</sup> and where  $p_0 N_D = n_i^2$ . In this way, the range of values taken by the observed lifetime can be readily determined. The three curves correspond to  $\tau_p$  values of 5, 50, and 100 ns. The majority carrier lifetime  $\tau_n$  is always taken to be 10 times  $\tau_p$  and  $N_D = 2 \times 10^{17} \text{ cm}^{-3}$ .

The progress of the TPL experiment for the case of  $\tau_p = 5 \text{ ns}$  can be traced along the solid line, as follows, in Fig. 11. Before the laser pulse occurs, the minority carrier density  $p$  has its equilibrium value which is approximately zero for these n-type samples. As the laser pulse excites the sample, creating electron-hole pairs,  $p$  increases, moving along the solid curve to the right. Near the peak of the laser pulse,  $p$  will take on its largest value. This value will depend on the laser pulse energy and duration. At this time, the carrier distribution in the sample is highly nonuniform, being determined by the complex interplay of the optical absorption length and the carrier concentration-dependent recombination processes. The location in the sample where the maximum carrier density occurs is undoubtedly near the illuminated surface and at the peak of the Gaussian spatial profile of the pulse. The value of this maximum saturates, as shown in Fig. 5, at the carrier density where  $G = R_{\text{tot}}$ , i.e., the combined recombination rate is equal to the generation rate. This carrier density can be computed to be about  $2.5 \times 10^{19} \text{ cm}^{-3}$  for the parameter values selected. Once this carrier

density is reached, as many carriers are recombining per unit time as are being generated. At this time,  $\tau_{\text{eff}}$  is very short due to the high value of  $R_{\text{BB}}$ . These conditions cause the high initial slope in the experimental decay curve shown in Fig. 1.

During the first few nanoseconds following the laser pulse,  $p$  decreases rapidly and the solid curve in Fig. 11 is traced back to the left. The value of  $\tau_{\text{eff}}$  is seen to increase to a maximum value, corresponding to the plateau in the experimental TPL curve in TD2. The previous discussion of Eqs. (2) and (3) and the analysis presented by Ahrenkiel and coworkers<sup>5</sup> suggested that this maximum should be  $\tau_n + \tau_p$ . The conditions of the solid line simulation are such that  $\tau_n + \tau_p = 55$  ns, yet it is clear that the maximum value of  $\tau_{\text{eff}}$  is approximately 10 ns. At later times when  $p$  is smaller,  $\tau_{\text{eff}}$  does not exactly equal  $\tau_p$ . In the solid line case,  $\tau_{\text{eff}} = 4.17$  ns, while  $\tau_p = 5$  ns. Thus, it must be concluded that even in  $\text{Al}_x\text{Ga}_{1-x}\text{As}$  and GaAs samples with  $\tau_p$  as short as 5 ns, BB recombination will prevent both the observation of  $\tau_p$  and  $\tau_n + \tau_p$  in the decay curve.

The dotted and dot-dashed lines in Fig. 11 correspond to samples with minority carrier lifetimes of 50 ns and 100 ns, respectively, which are more nearly equal to those achieved in state-of-the-art MOCVD samples. In these cases, the role of BB processes in determining  $\tau_{\text{eff}}$  is even greater. For a sample with  $\tau_p = 50$  ns and  $\tau_n = 500$  ns, the corresponding  $\tau_{\text{eff}}$  at low  $p$  is 16.7 ns, while the high  $p$  limit is approximately 18 ns instead of 550 ns. For a sample with  $\tau_p = 100$  ns and  $\tau_n = 1000$  ns, the corresponding  $\tau_{\text{eff}}$  at low  $p$  is 20 ns, while the high  $p$  limit is approximately 18 ns instead of 1100 ns. Therefore, in higher quality samples where the SRH lifetimes are larger, the BB processes must be included in the model. Furthermore, in these high quality samples, extraction of the minority carrier lifetime from samples dominated by BB recombination may be problematical.

A different representation of these results is given in Fig. 12. Here, the rates  $R_{\text{SRH}}$ ,  $R_{\text{BB}}$ , and  $R_{\text{Auger}}$  are plotted as functions of the same  $p$  as in Fig. 11. The solid lines correspond to the BB and Auger rates. The three broken curves correspond to the SRH rates for the three lifetime cases shown in Fig. 11, i. e., minority carrier lifetimes of 5 nsec, 50 nsec, and 100 nsec. Comparing the BB rate to the SRH rate for the 5 nsec minority carrier lifetime (dash-dotted line), it is clearly seen that for  $\Delta p > 1 \times 10^{17} \text{ cm}^{-3}$ ,  $R_{\text{BB}}$  is dominant and that Auger does not dominate until  $\Delta p > 5 \times 10^{19} \text{ cm}^{-3}$ . However, this is in the regime where the BB process is second order, as revealed by the slope of 2. By the time  $p$  has decreased

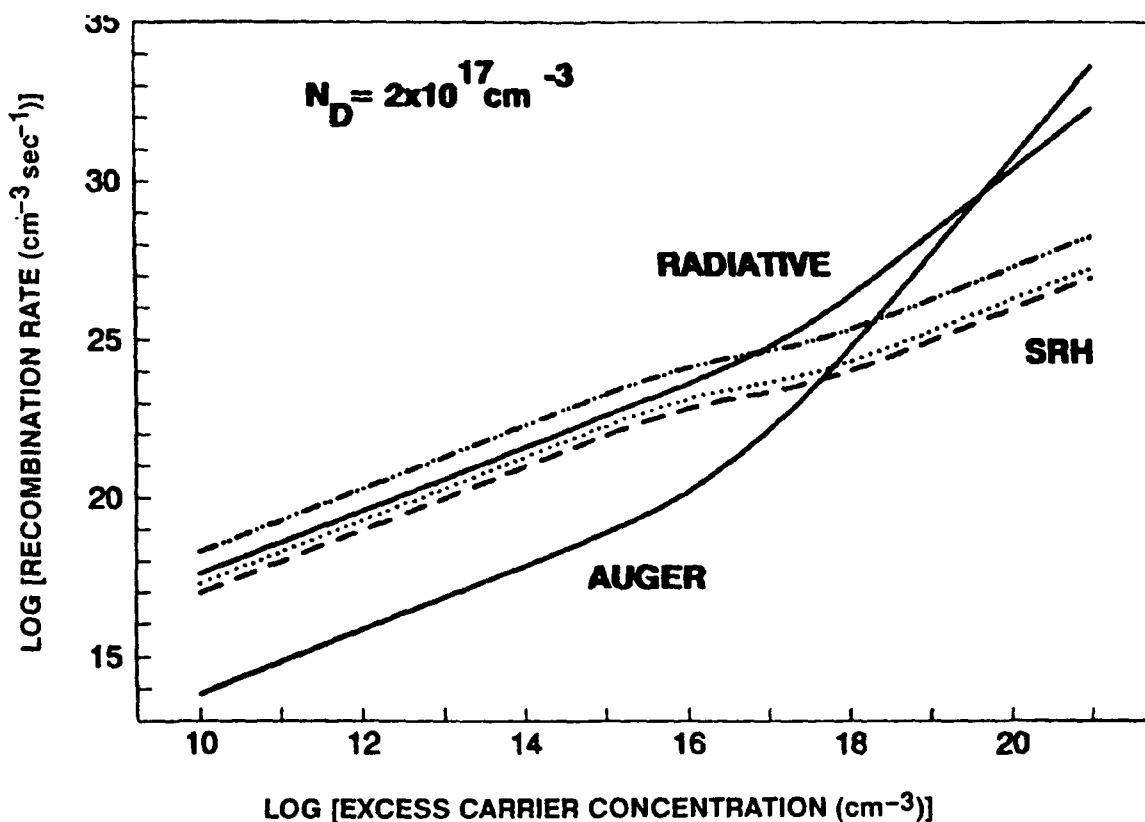


Figure 12. Band-to-band, (solid line) Shockley-Read-Hall (SRH), and Auger (solid line) recombination rates as a function of the maximum minority carrier density in the sample, for three different minority carrier lifetimes of 5 nsec, (SRH dash-dotted line) 50 nsec (SRH dotted line), and 100 nsec (SRH dashed line).  $N_D = 2 \times 10^{17} \text{ cm}^{-3}$ .

sufficiently that the BB process is pseudo-first order, the rate  $R_{BB}$  has become smaller than, but comparable, to  $R_{SRH}$ . Note that for the other two cases considered, i. e., minority carrier lifetimes of 50 ns and 100 ns, the BB rate is always larger than the SRH rates (dotted and dashed curves, respectively). Another way of displaying these same features is shown in Fig. 13, where we plot the Auger and BB lifetimes (solid lines) along with the SRH lifetimes for these same three cases. The only situation in which the BB effects will be negligible is in low doped samples where the BB lifetime computed from Eq. (1) is too long for the BB process to compete with the SRH relaxation.

In Fig. 14, we show the results of a simulation similar to that in Fig. 11, except that  $N_D = 1 \times 10^{14} \text{ cm}^{-3}$  instead of  $2 \times 10^{17} \text{ cm}^{-3}$ . The limiting  $\tau_{eff}$  values are seen to closely approximate  $\tau_p$  in the low p regime. However, in the high p regime, the limit  $(\tau_n + \tau_p)$  is not reached, even though  $\tau_{BB} = 50 \text{ } \mu\text{sec}$  and  $\tau_{Auger} = 556 \text{ sec}$ . In Fig. 15, we show the results of a simulation of the recombination rates similar to that in Fig. 12, and in Fig. 16, we show the results of a simulation of the effective lifetimes of the BB, Auger, and SRH processes similar to those in Fig. 13. Note here, however, that the SRH rates for all three cases are substantially larger than the BB or Auger rates at low values of  $\Delta p$ , and correspondingly, the SRH lifetimes are shorter than the BB and Auger lifetimes. However, because of the low value of  $N_D$ , the SRH rates do not take on their low density values until  $\Delta p < 1 \times 10^{13} \text{ cm}^{-3}$ . In measurements limited by signal-to-noise considerations, the lifetime at these low carrier densities may not be observable.

Figure 17 displays results of several simulations in which  $\tau_p$  is kept fixed at 5 ns and  $\tau_n$  is varied parametrically from 25 to 500 ns, for (a)  $N_D = 2 \times 10^{17} \text{ cm}^{-3}$  and (b)  $N_D = 1 \times 10^{14} \text{ cm}^{-3}$ . We note that, as before, at no carrier density does the carrier lifetime become  $\tau_n + \tau_p$ . Furthermore, these results show that longer majority carrier lifetimes can extend the time required for the asymptotic decay regime to be reached. This length of time is an important experimental consideration because the PL emission intensity is dropping exponentially with time. A long delay in reaching a single exponential decay can result in an unusable signal-to-noise ratio.

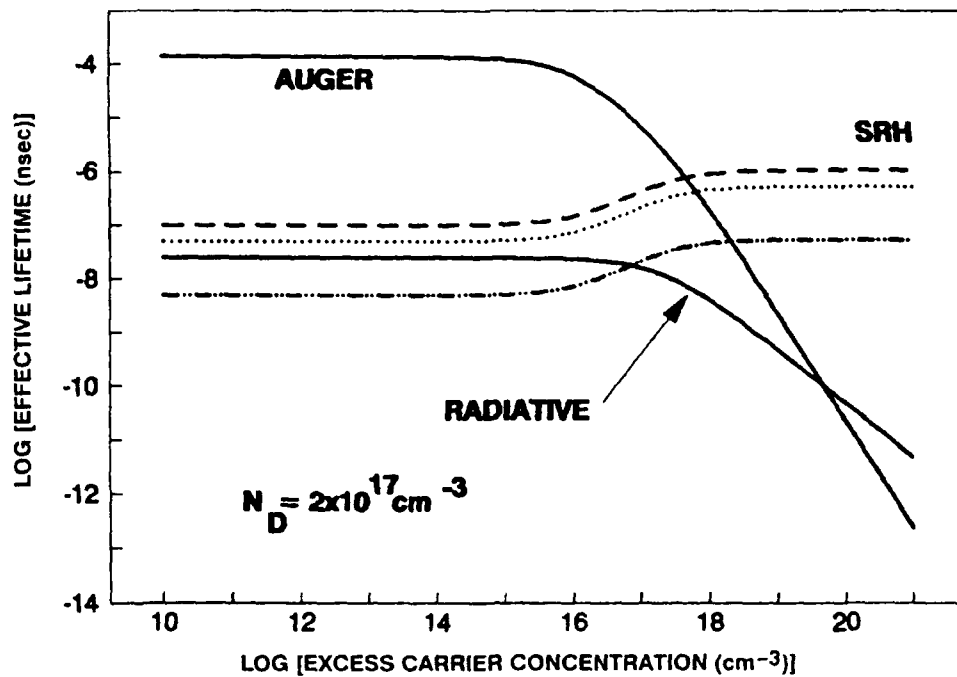


Figure 13. Band-to-band (solid line) Shockley-Read-Hall, and Auger (solid line) effective lifetimes as a function of the maximum minority carrier density in the sample, for three different minority carrier lifetimes of 5 nsec (SRH dot-dashed), 50 nsec (SRH dotted line), and 100 nsec (SRH dashed line).  $N_D = 2 \times 10^{17} \text{ cm}^{-3}$ .

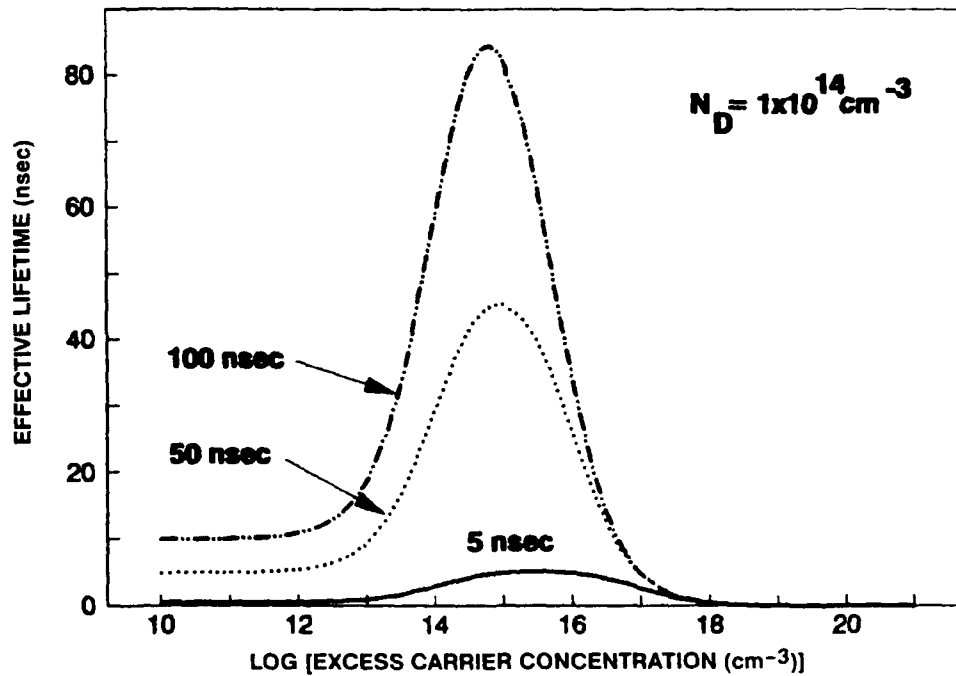


Figure 14. Same as Figure 11, except that equilibrium carrier concentration in sample is  $1 \times 10^{14}$  instead of  $2 \times 10^{17} \text{ cm}^{-3}$ .

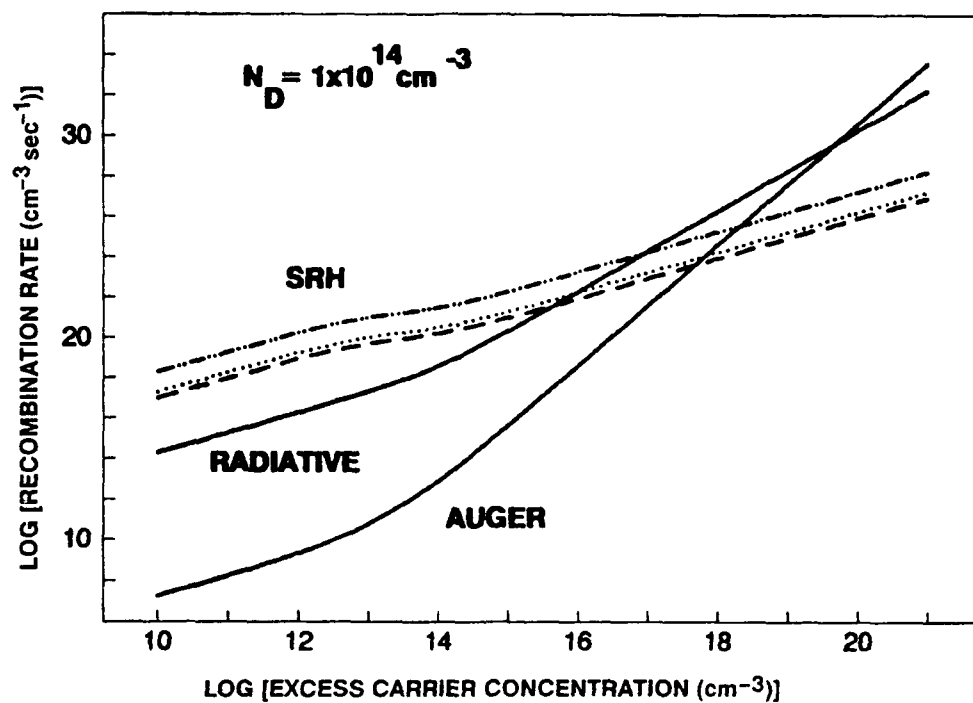


Figure 15. Same as Figure 12, except that equilibrium carrier concentration in sample is  $1 \times 10^{14}$  instead of  $2 \times 10^{17} \text{ cm}^{-3}$ .

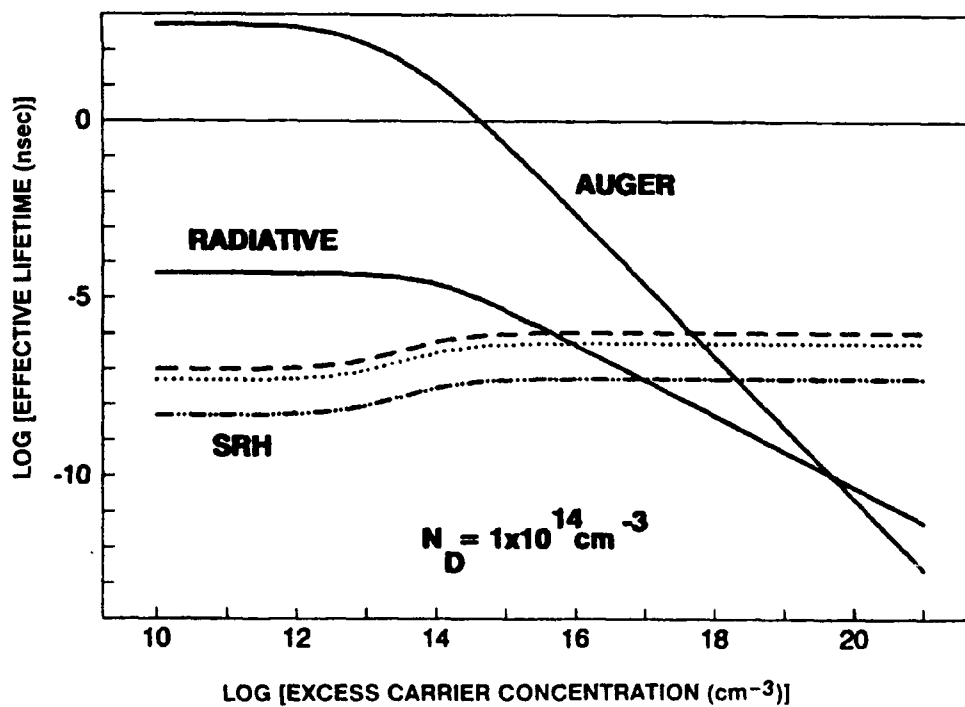
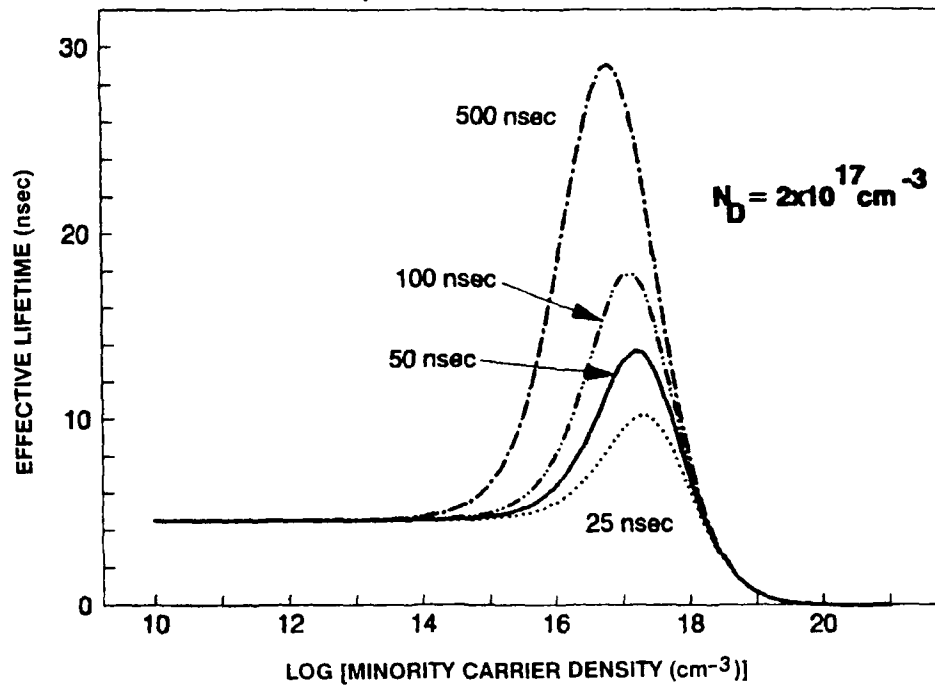
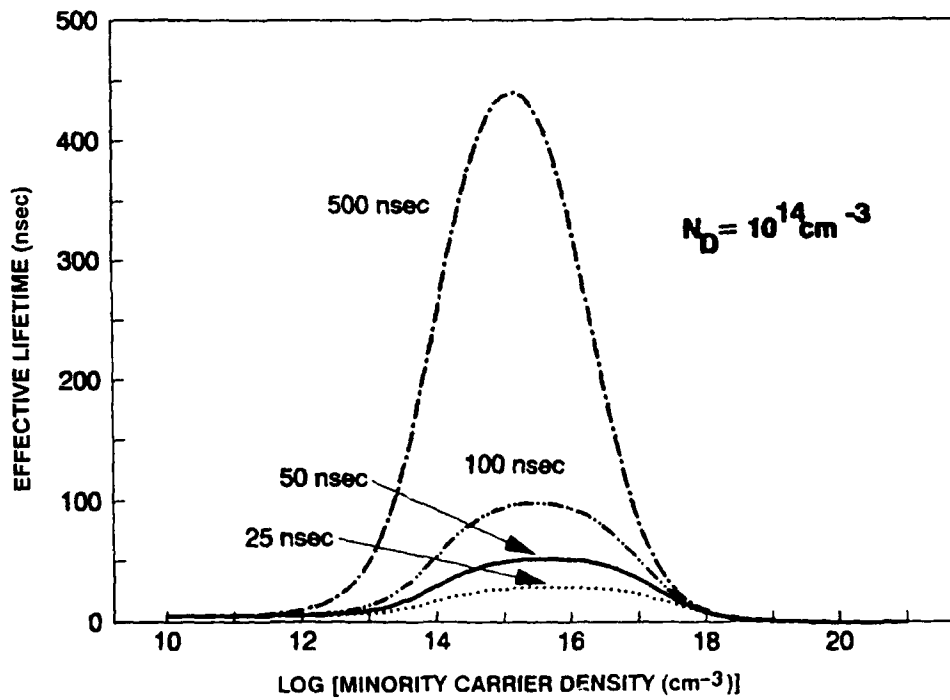


Figure 16. Same as Figure 13, except that equilibrium carrier concentration in sample is  $1 \times 10^{14}$  instead of  $2 \times 10^{17} \text{ cm}^{-3}$ .



(a)



(b)

Figure 17. Same as Figure 11, except that minority carrier lifetime is kept fixed at 5 nsec and majority carrier lifetime is varied as shown: (a)  $N_D = 2 \times 10^{17} \text{ cm}^{-3}$  and (b)  $N_D = 1 \times 10^{14} \text{ cm}^{-3}$ .



### III. DISCUSSION

The basic formulation of these recombination processes has been available for some time.<sup>4</sup> However, they have been applied recently in a confusing and inconsistent fashion. The inconsistencies and confusion in the analysis of TPL results are best shown by discussion of some specific examples. These examples are not the only cases where recombination analysis has been misapplied, but they serve to illustrate the points made above.

As we mentioned in the introduction, recent measurements of the minority carrier lifetime in AlGaAs SHs were performed using the slope extraction technique.<sup>3</sup> The analysis of these results attempted to incorporate the saturation of the SRH process properly. However, the analysis did not carefully consider the effective saturation of the carrier density in TD2 due to the initial rapid BB recombination in TD1. Because of this effective saturation, it may not be possible to obtain carrier densities within TD2 such that  $\Delta p \ll N_D$ . Consequently, the majority carrier lifetimes extracted from these results may be substantially in error. Furthermore, the analysis neglected the effects of BB recombination. Thus, in principle, the minority carrier lifetimes extracted from these results must be corrected to account for BB recombination. However, the BB lifetimes at these doping densities are much longer than the extracted minority carrier lifetimes. Consequently, we estimate the effects of neglecting BB recombination in extracting these minority carrier lifetimes to be, at most, a few percent. A careful analysis of the various measurements using numerical techniques similar to those described above would be required to accurately extract the correct minority and majority carrier lifetimes.

Recently, TPL measurements have been reported on p-GaAs DHs with doping densities ranging from  $10^{15}$  to  $10^{19} \text{ cm}^{-3}$ .<sup>23</sup> Excitation levels were approximately  $10^{14} \text{ cm}^{-3}$ . Consequently, these measurements were interpreted as having been performed in the low excitation regime in which the radiative relaxation is pseudo-first-order and the SRH lifetime is the minority carrier lifetime  $\tau_n$ . As is discussed above, this is valid as long as the majority carrier lifetime is no more than ten times the minority carrier lifetime. Furthermore, the TPL results are single exponential decays across the entire time domain of the measurements, which is an indicator of the low excitation regime. Lifetimes were extracted using the slope extraction technique. Interface recombination and photon recycling effects are also included in

the analysis. Thus, the lifetimes extracted from the analysis are obtained in a manner consistent with proper analysis as described above.

The slope extraction technique was also recently used to determine minority carrier lifetimes from AlGaAs alloys.<sup>13</sup> An effective lifetime was extracted and related to the minority carrier lifetime by taking into consideration surface or interface recombination effects. However, it is not clear from the presentation within which time domain the lifetime is extracted. In TD1, the TPL measurements show the rapid relaxation which is clearly identified with nonlinear recombination phenomena. Furthermore, the competing effects of SRH, BB, and Auger recombination were not taken into account. Thus, the true minority carrier lifetime does not emerge from the analysis.

TPL measurements have recently been reported for n-Al<sub>0.38</sub>Ga<sub>0.62</sub>As SHs and DHs.<sup>2</sup> These data were analyzed on the basis of an analytical solution to the one-dimensional diffusion equation which incorporates recombination as simply  $\Delta p/\tau$ . As we have shown above, this analysis requires extraction of the minority carrier lifetime from an effective linearized lifetime that includes the competing effects of the SRH, BB, and Auger processes. Furthermore, this analysis is only valid for the low excitation regime in which  $\Delta p \ll N_D$ . However, laser pulses with a fluence at the sample of about 0.1 mJ/cm<sup>2</sup> were used. For this alloy, the absorption coefficient is larger than  $2 \times 10^4$  cm<sup>-1</sup> for an absorption depth of less than 0.5  $\mu$ m. At these fluences, the photoexcited carrier densities will at least be comparable to the doping levels of their samples, which range from  $4 \times 10^{15}$  to  $4 \times 10^{16}$  cm<sup>-3</sup>. Consequently, a proper analysis of these results would at least require inclusion of the saturation of the SRH process.

TPL measurements have also recently been reported for p-GaAs DHs.<sup>7</sup> Lifetimes were extracted from these results with a fit using an analytical solution in the form of a Fourier series solution to the transient diffusion equation. The recombination in this model is linearized to the form  $\Delta n/\tau$ . In these results, the lifetime is a combination of a nonradiative component (SRH) and a radiative component. However, the nonradiative component of the lifetime is treated as a constant, independent of carrier density. As we have seen, SRH recombination has a complicated nonlinear dependence on intensity unless the TPL measurements are performed in the regime in which  $\Delta n \ll N_A$ . From the qualitative features of these TPL results, it is clear that during TD1, nonlinear recombination effects

dominate the response. However, it is not clear that the exponential region from which the lifetimes were extracted is TD3. It is likely that these lifetimes have been extracted from TD2, in which case a more complete formulation of the recombination problem must be performed in order to extract meaningful lifetimes.

TPL measurements have also recently been reported for n-GaAs and n-Al<sub>1-x</sub>Ga<sub>x</sub>As DHs.<sup>5</sup> In this work, the importance of including radiative recombination in the analysis of typical TPL measurements is acknowledged, but the authors assert that the measurements were performed on samples in which SRH effects dominate. The recombination effects model based solely on the SRH process as described in the previous section was used to extract both minority and majority carrier lifetimes. As we have shown in the previous section, this is not generally valid.

In more recent work, TPL measurements were performed on n-GaAs DHs.<sup>6</sup> TPL measurements were performed for a variety of sample thicknesses ranging from 0.25 to 10  $\mu\text{m}$ . The doping levels were relatively high ( $1.3 \times 10^{17} < N_D < 3.8 \times 10^{18} \text{ cm}^{-3}$ ). The measured lifetime is described in terms of an effective lifetime incorporating SRH, BB, and Auger effects as well as surface recombination. For the intensities used, it seems likely that the measurements were performed in the low excitation regime, so that the SRH lifetime is equal to the minority carrier lifetime. From the analysis, a slight dependence of the BB recombination coefficient B on the doping level was deduced. This has been previously discussed by Gershenzon, who concluded that such a dependence is not reasonable.<sup>29</sup> A possible complication of these results is that the Al<sub>1-x</sub>Ga<sub>x</sub>As layers used for passivation and confinement are Al<sub>0.3</sub>Ga<sub>0.7</sub>As, which has significant absorption at the 600 nm excitation wavelength. This would produce carriers in the Al<sub>0.3</sub>Ga<sub>0.7</sub>As layers and would reduce the carrier density within the GaAs active region. The resulting carrier dynamics could be substantially influenced by carrier transport and recombination at the interfaces. A further complication comes from the fact that the luminescence comes from a photoexcited n-GaAs DH fabricated on a p-GaAs substrate. Consequently, for the thinner structures, it is highly likely that some luminescence from the substrate and the p-GaAs buffer layer is observed.

TPL techniques have also been used to investigate the carrier recombination dynamics of a number of Cr-doped GaAs samples.<sup>19</sup> The results were analyzed in terms of a one-dimensional model similar to Eqs. (1)-(5) above, with the recombination term treated as

simply  $\Delta p/\tau$ . In this model, the samples were treated as semi-infinite slabs. This leads to an analytical solution of the carrier evolution equation. However, good fits to the results were not obtained using commonly accepted values for the diffusion coefficient and surface recombination velocity. Capture cross sections were deduced from the measured lifetimes and the known dopant densities. However, the extracted cross sections were not self-consistent over the range of samples investigated. These inconsistencies are most likely due to the fact that this formulation of the carrier recombination problem does not properly incorporate the effects of the competing SRH, BB, and Auger recombination processes. The short lifetimes that reported for these samples are consistent with the nonlinear processes that occur in TD1.

An electro-optical cross-correlation technique similar to the TPL technique has recently been used to measure the carrier recombination dynamics in GaAs/AlGaAs superlattice structures.<sup>20</sup> The results were analyzed using a similar analytical solution with carrier recombination linearized as  $\Delta n/\tau$ . The lifetimes extracted from such analysis are at best effective lifetimes incorporating the competing effects of SRH, BB, and Auger recombination. However, the excitation levels in these measurements were large enough that the photoexcited carrier densities are larger than the doping levels. Clearly, under these circumstances, a more detailed model must be used to properly incorporate the nonlinear recombination processes.

TPL measurements have also recently been performed upon a variety of multi-quantum well structures.<sup>24</sup> The active regions in these structures had well thicknesses of less than 20 nm. Consequently, other physical phenomena than those incorporated into our discussion may play a role in these results. Nonetheless, the measured TPL curves display features consistent with the TD1, TD2, and TD3 regions described above and are observed to depend strongly upon increasing excitation. The lifetimes extracted from these measurements were probably taken from TD2. Consequently, the extracted lifetimes would not be the minority carrier lifetime, nor could the minority carrier lifetime be extracted from such information.

Finally, we note that the conclusions drawn above concerning TPL measurements may also impact other measurements of photogenerated effects in semiconductor materials and devices. Recently, zero field time-of-flight measurements have been performed upon p-type C- doped GaAs samples.<sup>31</sup> A model was developed for evaluating the transient voltage pulse produced in the sample. The analysis consisted of an equivalent circuit model incorporating the evolution of the photogenerated carriers with a carrier evolution model similar to Eqs. (1)-

(5) above. The model has nine parameters, of which only the diffusion coefficient and the "carrier lifetime" were treated as free parameters. The result of this analysis yields an analytical solution to the problem in the form of an infinite series. However, in order to obtain this analytical result, the analysis of the recombination processes involved in these samples approximates the recombination rate as  $\Delta n/\tau$ . Clearly, considering the analysis provided above, it is evident that the lifetimes extracted from these results are not the minority carrier lifetimes. Even if the carrier densities were low enough that  $\Delta n \ll N_A$ , then the extracted lifetime would not be the minority carrier lifetime  $\tau_n$ , but would be

$$1/\tau = 1/\tau_n + B N_A + C_p N_A^2 . \quad (17)$$

Applying such analysis to the values extracted for  $\tau_n$  of 0.17, 0.45, and 2.0 nsec from the room temperature results, we obtain values of 0.33, 1.1, and 7.9 nsec for the minority carrier lifetime. We emphasize, however, that this result can only be meaningful if the excess carrier densities in the samples during these measurements are less than the number of carriers initially in the sample due to the dopants. Otherwise, it is impossible to extract the minority carrier lifetimes without a detailed fit to the results using a model that treats the recombination processes more accurately. The authors do not provide estimates of the carrier concentrations produced in the samples during the photogenerated transients. Consequently, the accuracy of this evaluation cannot be verified.

#### IV. CONCLUSIONS

We have compared and contrasted different methods of analyzing TPL measurements. From our analysis of the recombination processes associated with TPL measurements, we can draw the following conclusions.

1. The effective lifetimes extracted from the slopes of TPL curves do not, in general, correspond to any single physical lifetime such as the minority carrier lifetime.
2. In general, it is not possible to extract the minority carrier lifetime from a single TPL measurement. It is possible to extract the minority carrier lifetime from a single TPL measurement if (a) the optical intensity of the excitation pulse is low enough so that nonlinear BB and SRH recombination effects do not distort the TPL transient and if (b) the radiative recombination coefficient, the Auger recombination coefficient, the donor density (for n-type samples), and the interface recombination velocities are accurately known.
3. The slopes of the TPL curves in TD2 described in the introduction do not, in general, correspond to the sum of the minority carrier and majority carrier lifetimes as suggested by Ahrenkiel and coworkers.<sup>5</sup>
4. The generalized recombination analysis performed by some workers, in which the recombination rate is approximated as  $\Delta p/\tau$ , is not meaningful unless the carrier densities produced in the sample are accurately known and the fundamental parameters described in (2) above are accurately known.
5. Saturation of the SRH centers can cause BB recombination to dominate even when  $\tau_p < \tau_{BB}$  if  $\tau_n < \tau_{BB}$ .
6. At very high excitation levels, nonlinear recombination rapidly reduces the photoluminescence. Within TD2 and TD3, TPL curves produced at these excitation levels appear to be independent of excitation intensity. An aspect of this phenomenon is that since the observed decay curve will appear to be independent of excitation level, this might be mistaken for the low excitation limit. Thus, the response within the first few nanoseconds of excitation must be carefully examined.

Consequently, for samples where the conditions outlined in (2) above are not met, a series of measurements over a range of intensities, followed by detailed analysis using

numerical techniques similar to those outlined above, will be required to extract the desired parameters. In order for the analysis to be effective, the excitation levels must also be accurately known.

## REFERENCES

1. D. V. O'Connor and D. Phillips, *Time-Correlated Single Photon Counting* (Academic Press, New York, 1984).
2. R. K. Ahrenkiel, D. J. Dunlavy, R. Y. Loo, and G. S. Kamath, *J. Appl. Phys.* **63**, 5174 (1988).
3. D. C. Marvin and L. F. Halle, Proc. 21st IEE Photovoltaic Specialists Conf. (IEEE, New York, 1990), Vol. 1, p. 353.
4. J. S. Blakemore, *Semiconductor Statistics* (Pergamon Press, Oxford, 1962).
5. R. K. Ahrenkiel, B. M. Keyes, and D. J. Dunlavy, *Solar Cells* **30**, 163 (1991); and *J. Appl. Phys.* **70**, 225 (1991).
6. G. B. Lush, H. F. McMillan, B. M. Keyes, R. K. Ahrenkiel, M. R. Melloch, and M. S. Lundstrom (to be published).
7. R. K. Ahrenkiel, D. J. Dunlavy, J. Benner, R. P. Gale, R. W. McClelland, J. V. Gormley, and B. D. King, *Appl. Phys. Lett.* **53**, 598 (1988).
8. D. J. Wofford, G. D. Gilliland, T. F. Kuech, L. M. Smith, J. Martinsen, J. A. Bradley, C. F. Tsang, R. Venkatasubramanian, S. K. Ghandi, and H. P. Hjalmarson, *J. Vac. Sci. Technol. B* **9**, 2369 (1991).
9. S. A. Ringel and A. Rohatgi, *IEEE Trans. Electron Devices* *ED-38*, 2402 (1991).
10. L. M. Smith, D. J. Wofford, J. Martinsen, R. Venkatasubramanian, and S. K. Ghandi, *J. Vac. Sci. Technol. B* **8**, 787 (1990).
11. L. M. Smith, D. J. Wofford, R. Venkatasubramanian, and S. K. Ghandi, *Mat. Res. Soc. Proc.* **163**, 95 (1990).
12. J. P. Bergman, Q. X. Zhao, P.-O. Holtz, B. Monemar, M. Sundaram, J. L. Merz, and A. C. Gossard, *Mat. Res. Soc. Proc.* **160**, 703 (1990).
13. M. L. Timmons, J. A. Hutchby, R. K. Ahrenkiel, and D. J. Dunlavy, Proc. Int. Symp. GaAs and Related Compounds (1988), p. 289.
14. M. Gurioli, A. Vinattieri, M. Colocci, C. Deparis, J. Massies, G. Neu, A. Bossacchi, and S. Franchi, *Phys. Rev. B* **44**, 3115 (1991).



15. G. D. Gilliland, D. J. Wofford, T. F. Kuech, and J. A. Bradley, *J. Vac. Sci. Technol. B* **9**, 2377 (1991).
16. A. F. Dite, I. V. Kukushkin, V. B. Timofeev, A. I. Filin, and K. von Klitzing, *JETP Lett.* **54**, 389 (1991).
17. H. Hillmer, A. Forchel, T. Kuhn, G. Mahler, and H. P. Meier, *Phys. Rev. B* **43**, 13992 (1991).
18. S. Charbonneau, J. F. Young, and A. J. Springthorpe, *Proc. SPIE* **1283**, 23 (1990).
19. J. S. Weiner and P. Y. Yu, *J. Appl. Phys.* **55**, 3889 (1984).
20. J. Puls, F. Henneberger, I. N. Uraltsev, and A. M. Vasiliev, *Superlattices and Microstructures* **9**, 503 (1991).
21. A. Von Lehman and J. M. Ballantyne, *J. Appl. Phys.* **58**, 958 (1985).
22. C. Lopex, F. Meseguer, J. Sanchez-Dehesa, W. W. Ruhle, and K. Ploog, *Proc. SPIE* **1361**, 89 (1990).
23. R. J. Nelson and R. G. Sobers *J. Appl. Phys.* **49**, 6103 (1978).
24. A. Hariz, P. D. Dapkus, H. C. Lee, E. P. Menu, and S. P. DenBaars, *Appl. Phys. Lett.* **54**, 635 (1989).
25. M. ettenberg and H. Kressel, *J. Appl. Phys.* **47**, 1538 (1976).
26. E. H. C. Parker, Ed., *The Technology and Physics of Molecular Beam Epitaxy* (Plenum Press, New York, 1983).
27. E. D. Palik, in *Handbook of Optical Constants of Solids*, edited by E. D. Palik (Academic Press, New York, 1985), pp. 429-443.
28. O. J. Glembocki and K. Takarabe, in *Handbook of Optical Constants of Solids II*, edited by E. D. Palik (Academic Press, New York, 1991), pp. 513-558.
29. M. Gershenzon, in *Semiconductors and Semimetals, Physics of II-V Compounds*, edited by R. K. Willardson and A. C. Beer (Academic Press, New York, 1966), Vol. 2, Chapt. 13, pp. 289-369.
30. M. Takeshima, *J. Appl. Phys.* **58**, 3846 (1985).
31. C. M. Colomb, S. A. Stockman, S. Varadarajan, and G. Stillman, *Appl. Phys. Lett.* **60**, 65 (1992).

# APPENDIX

## SIGNAL-TO-NOISE RATIO AND DYNAMIC RANGE OF TRANSIENT PHOTOLUMINESCENCE MEASUREMENTS AT LARGE SPOT SIZE AND LOW EXCITATION LEVEL.

If one photoexcites a double heterostructure (DH) at a low enough excitation level, one can stay in the regime where the recombination rate is quasi-linear. In this regime, for an n-type sample, the lifetime is given by

$$1/\tau_{\text{eff}} = 1/\tau_p + BN_D + C_n N_D^2, \quad (\text{A1})$$

where  $\tau_p$  is the minority carrier lifetime,  $B$  is the radiative recombination coefficient,  $N_D$  is the number of donor electrons, and  $C_n$  is the Auger recombination coefficient for the electron-electron-hole process. Can one stay in this regime and detect a signal using standard TPL measurement techniques?

In this regime, the radiative recombination rate is

$$R_{\text{rad}} = BN_D p(x,y,z,t), \quad (\text{A2})$$

where  $p(x,y,z,t)$  is the excess minority carrier density within the sample. The total number of photons emitted from the sample per unit time is the integral over the photoexcited volume of the radiative recombination rate. Consequently, if  $p(x,y,z,t)$  is small, the radiative rate is small. This may cause detection problems if one is limited by signal-to-noise considerations.

One possible solution is to use a fairly energetic laser pulse in conjunction with large spot sizes. With a large enough spot size, one can keep the energy density in the photoexcited volume low enough that one can stay in the quasilinear regime. Furthermore, there should be plenty of signal, providing that one can collect a substantial portion of the light emitted from the sample.

Consider a uniformly illuminated disk of volume

$$V = \pi r^2 L, \quad (\text{A3})$$

where  $r$  is the radius of the photoexcited volume and  $L$  is its thickness. Assume that  $N_D = 1 \times 10^{14} \text{ cm}^{-3}$  and that we wish to keep  $p(x,y,z,t) < N_D$ . The number of photons radiated per unit time is

$$N_p = VR_{\text{rad}} = \pi r^2 L B N_D p(x,y,z,t). \quad (\text{A4})$$

The evolution of the excess carrier density under these conditions is given by

$$dp/dt = -p/\tau_{\text{eff}} \quad (\text{A5})$$

or

$$p(x,y,z,t) = p_0 \exp(-t/\tau_{\text{eff}}), \quad (\text{A6})$$

where  $p_0$  is the initial excess charge carrier density. Here, we have assumed that the excitation is a delta function compared to the decay and that diffusion and surface recombination do not affect these results. The total number of photons emitted over a time interval  $t = 0$  to  $t = T$  is given by the integral over the time interval of the number of photons emitted per unit time, i.e.,

$$N_p^{\text{tot}} = \pi r^2 L B N_D p_0 \tau_{\text{eff}} [1 - \exp(-T/\tau_{\text{eff}})]. \quad (\text{A7})$$

For  $T \gg \tau_{\text{eff}}$ , the quantity in brackets is approximately unity, so that

$$N_p^{\text{tot}} = \pi r^2 L B N_D p_0 \tau_{\text{eff}}. \quad (\text{A8})$$

Assuming that  $\tau_p = 5 \text{ nsec}$ ,  $B = 2 \times 10^{-10} \text{ cm}^3/\text{sec}$ , and  $C_n = 1.8 \times 10^{-31} \text{ cm}^6/\text{sec}$ ,  $\tau_{\text{eff}}$  is approximately equal to  $\tau_p$ .

The number of photons observed depends upon the collection efficiency of the apparatus. Assume that the emitted light is collected by a lens of diameter  $d$  placed a distance

D from the sample and that all of this light is sent into the detection apparatus, i.e., the monochromator and detector. Then the collection efficiency is

$$K = \gamma T_m (d/4D)^2 (1-R), \quad (A9)$$

where  $T_m$  is the transmittance of the monochromator,  $R$  is the reflectivity of the semiconductor material at the wavelength of the emitted photons, and  $\gamma$  is the quantum efficiency of the detector. Assume that  $T_m = 0.1$ ,  $R = 0.35$  and that  $\gamma = 0.25$ . Further, assume that our apparatus has a 2 in. diameter lens placed 6 in. from the sample. Consequently,  $K = 1.13 \times 10^{-4}$ . The number of photons collected is

$$N_p^c = K N_p^{\text{tot}}. \quad (A10)$$

For a spot 5 mm in radius and a DH thickness of 5  $\mu\text{m}$ , and for  $\tau_p = 5$  nsec, we obtain 44 photons of signal from each excitation pulse. One would like to keep the count rate at about 0.01 photons per pulse to ensure the validity of the time-correlated single photon counting technique.<sup>1</sup> Consequently, it seems that there is plenty of signal to perform TPL measurements this way.

In order to photogenerate  $10^{13}$  carriers  $\text{cm}^{-3}$  in the indicated volume, one needs approximately  $6 \times 10^9$  photons in a pulse. At the laser wavelength of 590 nm, this corresponds to approximately 2 nJ per pulse. At a repetition rate of 400 kHz, this corresponds to an average power of 0.8 mW.

At long times after excitation, the count rate will fall off substantially. The total number of photons emitted over a time interval  $t = T_1$  to  $t = T_2$  is given by the integral over the time interval of the number of photons emitted per unit time, i. e.,

$$N_p^{\text{tot}} = \pi^2 L B N_D p_0 \tau_{\text{eff}} [\exp(-T_1/\tau_{\text{eff}}) - \exp(-T_2/\tau_{\text{eff}})]. \quad (A11)$$

The total number of photons emitted during the period from  $t = T_1$  to  $t = \text{infinity}$  is given by

$$N_p^{\text{tot}} = \pi^2 L B N_D p_0 \tau_{\text{eff}} \exp(-T_1/\tau_{\text{eff}}). \quad (A12)$$

The signal has decayed by four orders of magnitude when  $t > 9 \tau_{\text{eff}}$ . For the parameters given above, this corresponds to  $T_1 = 45$  nsec. Including the collection efficiency calculated above, we obtain  $5.5 \times 10^{-3}$  counts per pulse in the time interval beyond 45 nsec. For a five minute counting interval at a repetition rate of 400 kHz, this corresponds to 650,000 counts. Most of these occur within the time interval from  $t = 45$  nsec to  $t = 90$  nsec, with only 81 counts over the entire time interval after 90 nsec. Consequently, we estimate that the dynamic range of this technique is somewhere between four to eight orders of magnitude for these parameters.